EUROPEAN COMMISSION

Community Research

SEVENTH FRAMEWORK PROGRAMME

CARBOWASTE

Treatment and Disposal of Irradiated Graphite and Other Carbonaceous Waste

Grant Agreement Number: FP7-211333

- Technical Report (WP 6 Task 1) – BEHAVIOUR OF RADIONUCLIDES IN UNGG GRAPHITE IN AQUEOUS MEDIA State-Of-The-Art Review

Author(s): **CEA & Andra**

Reporting period: e.g. 01/04/2010-01/04/2011

Date of issue of this report : 30/03/2011

Start date of project : **01/04/2008** Duration : **48 Months**

Project co-funded by the European Commission under the Seventh Framework Programme (2007 to 2011) of the European Atomic Energy Community (EURATOM) for nuclear research and training activities		
Dissemination Level		
PU	Public	
RE	Restricted to the partners of the CARBOWASTE project	
CO	Confidential, only for specific distribution list defined on this document	**X**

Distribution list

Person and organisation name and/or group	Comments
W. Von Lensa CARBOWASTE Project Coordinator	
B. Grambow, WP6 leader	
CARBOWASTE beneficiaries	

CARBOWASTE		
Work package: 6 **Task: :** 6.1	**CARBOWASTE document no:** CARBOWASTE-1103-D-WP6.Task.1 (e.g. May 2008 as date of issue: 0805)	**Document type:** D=Deliverable / M=Minutes / P=Progress report / T=Technical Report
Issued by: CEA - Andra **Internal no.:** Technical report CEA Behaviour of radionuclides in UNGG		**Document status:** Final

Document title

BEHAVIOUR OF RADIONUCLIDES IN UNGG GRAPHITE IN AQUEOUS MEDIA State-Of-The-Art Review

Executive summary

The first generation of French nuclear plants (9 UNGG reactors, Natural Uranium Graphite Gas) was operated from 1956 to 1994. This technology has generated large amounts of graphite waste - the current inventory is 23,000 tons – which are classified as a long-lived low-level waste. The long term radiological issue mainly relies on two radionuclides:

- Carbon 14, the main long-lived radionuclide in graphite waste
- Chlorine 36, the main potential contributor to the long term impact of graphite in disposal

Since the late 80's France has been conducting leaching experiments in order to predict the release of such radionuclides during under-water decommissioning and low-depth disposal. The present report is a state-of-the art review of data that have been collected within this framework. Studies deal with water penetration kinetics as well as with radionuclide behavior during leaching experiments. Concerning chlorine 36 it was found that its release fraction in aqueous solution range from 10 to 90 % depending on the thermal operating conditions. It is suggested that two forms of chlorine 36 may be present within graphite: a labile fraction which is weakly bound to graphite, and a complementary fraction that is slowly released and whose chemical form is less labile or whose localization within graphite porosity is less accessible to water.
On the contrary, the release kinetics of carbon 14 and tritium is found to be much lower than chlorine 36. Speciation was not characterized. Some results on ^{60}Co, ^{63}Ni, ^{133}Ba and ^{137}Cs are also summarized.

Revisions

Rev.	Date	Short description	Author	Internal Review	Task Leader	WP Leader
00	dd/mm/yyyy	Issue	Name, Organisation	Name, Organisation *Signature*	Name, Organisation *Signature*	Name, Organisation *Signature*
01	30/03/2011	First issue	J. Comte CEA	L. Petit Andra		B. Grambow Subatech

Contents

1 INTRODUCTION 8

2 PROPERTIES OF NUCLEAR GRAPHITE AND EVOLUTION UNDER IRRADIATION 10

2.1 STRUCTURE AND MANUFACTURING PROCESS 10

2.2 EFFECTS OF NEUTRON BOMBARDMENT 12

2.3 GRAPHITE OXIDATION 14

2.4 GRAPHITE POROSITY 16

2.4.1 Definition of the porosity scale 16

2.4.2 Porosity in non-irradiated graphite 17

2.4.3 Porosity in irradiated graphite 18

3 WATER PENETRATION INTO GRAPHITE 21

3.1 WATER VAPOR 21

3.2 IMMERSION TESTS 21

4 LEACHING BEHAVIOR OF GRAPHITE RADIONUCLIDES 25

4.1 DESCRIPTION OF STUDIES 25

4.2 BEHAVIOR OF ^{36}CL 28

4.2.1 Leaching of graphite from G2 and Hanford reactors 28

4.2.2 Other graphite leaching tests on G2 stack 32

4.2.3 Graphite leaching of Bugey 1 stack 34

4.2.4 Graphite leaching from sleeves in Saint-Laurent A2 39

4.2.5 Diffusion measurements of ^{36}Cl in G2 and Bugey 1 graphite 40

4.2.6 Conclusion on the behavior of ^{36}Cl 43

4.3 BEHAVIOR OF ^{3}H AND ^{14}C 43

4.3.1 Comparison of results for G2 and Hanford reactors 43

4.3.2 Leaching on G2 graphite stack 45

4.3.3 Graphite leaching on Bugey 1 stack 45

4.3.4 Graphite leaching from SLA2 sleeves 47

4.3.5 ^{3}H diffusion measurements in graphite 48

4.3.6 Conclusion on ^{3}H and ^{14}C leaching behavior 49

4.4 BEHAVIOR OF OTHER RADIONUCLIDES 49

4.4.1 Graphite leaching on G2 stack 49

4.4.2 Graphite leaching from Bugey 1 stack 50

4.4.3 Graphite leaching from SLA2 sleeves 51

4.4.4 Conclusion on the behavior of other radionuclides 52

5 CONCLUSION 53

6 REFERENCES 55

Figures

Figure 1 – Structure of graphite [2] 10
Figure 2 – Nuclear graphite manufacturing process [3]. 11
Figure 3 – Defects created during graphite irradiation by fast neutrons [3]. 12
Figure 4 - Wigner energy spectrum of graphite irradiated at 60°C under a neutron fluence of $1.67.10^{20}$ $n.cm^{-2}$ (or 0.12 displacements per atom) [4]. 13
Figure 5 - Porosity class thresholds [13]. 17
Figure 6 - Distribution of pore diameters for non irradiated graphite (G2 reactor). 18
Figure 7 - Variation in porosity as a function of the pore radius for two graphite samples (Lo.L coke): — non irradiated, - - - irradiated under He [18]. 19
Figure 8 - Variation in porosity as a function of the porous radius for two graphite samples (Lo. L coke): — non irradiated, - - - irradiated under CO_2 [18]. 20
Figure 9 – Evolution of the water adsorption rate of non irradiated graphite with time. 23
Figure 10 - Cumulative leached fraction of ^{36}Cl as a function of square root of time for G2 (core No.14) and Hanford (DIW-25) graphite samples (pure water, room temperature). 30
Figure 11 - Evolution of the cumulative leached fraction of ^{36}Cl with time (G2 reactor). 33
Figure 12 - Impact of experimental leaching conditions on the evolution of the cumulative released fraction of ^{36}Cl (09/17/2001) with time [29]. 35
Figure 13 - Cumulative released fraction of ^{36}Cl versus the initial activity in the sample (blocks and powder, from Table 9). 36
Figure 14 - Cumulative leach fraction of ^{36}Cl as a function of the position of graphite samples in the stack. 37
Figure 15 - Fraction of ^{36}Cl released into solution as a function of the position of graphite in the stack for solid and powder samples. 38
Figure 16 - ^{36}Cl cumulative leached fraction versus the square root of time for two SLA2 sleeves samples. 40
Figure 17 - Chlorine 36 released fraction and computed diffusion profile (solid line) in pure water. 41
Figure 18 - ^{36}Cl diffusion through a sample of non-irradiated G2 graphite. 42
Figure 19 - Cumulative leached fraction of ^{14}C versus time for G2 and Bugey samples. 47
Figure 20 - Tritium diffusion through a sample of non-irradiated graphite from G2 reactor. 49

Tables

Table 1 - Factors impacting graphite density loss [9]. 15
Table 2 - Percentage of mass increase in irradiated and non irradiated graphite samples [23]. 21
Table 3 - Characteristics of graphite samples used in the immersion tests. 22
Table 4 - Leaching conditions for graphite samples from Hanford, G2, SLA2 and Bugey1 reactors. 26
Table 5 - Cumulative leached activity of ^{36}Cl for G2 (1988) and Hanford (1987) reactors (PNL results). 29
Table 6 - Cumulative leached fraction of ^{36}Cl for G2 (09/01/1988) and Hanford (06/24/1989) reactors (CEA results). 30
Table 7 - Leaching results for G2 and influence of graphite mass. 31
Table 8 - Cumulative leached fraction of ^{36}Cl for G2 stack graphite (03/09/2004). 32
Table 9 - Cumulative leached fraction of ^{36}Cl for Bugey 1 graphite stack for solid (09/17/2001) and powder (05/23/2006) samples. 34
Table 10 - ^{36}Cl cumulative leached fraction for graphite samples from SLA2 sleeves (07/18/1997). 39
Table 11 - Diffusion coefficients fitted from tests on G2 and Bugey 1 graphite samples. 41
Table 12 –Cumulative leached fraction of ^{14}C for G2 (1988) and Hanford (1987) graphite samples (PNL results) 44
Table 13 – Cumulative leached fraction of ^{3}H and ^{14}C for G2 (09/01/1988) and Hanford (06/24/1989) samples (CEA results). 44
Table 14 – Cumulative leached fraction of ^{14}C and ^{3}H for G2 stack samples (03/09/2004). Values in blue are below the detection limit. 45
Table 15 - Cumulative leached fraction of ^{3}H and ^{14}C for Bugey 1 graphite on solid (09/17/2001) and powder (23/05/2006) samples. Values in blue are below the detection limit. 46
Table 16 - Cumulative leached fraction of ^{3}H and ^{14}C for SLA2 sleeves (07/18/2007). 48
Table 17 - Cumulative leached fraction of ^{60}Co, ^{63}Ni, ^{133}Ba and ^{137}Cs for G2 stack samples (03/09/2004) 49
Table 18 - Cumulative leached fraction of ^{60}Co, ^{137}Cs and ^{63}Ni from Bugey 1 stack block samples. 50
Table 19 - Cumulative leached fraction of ^{60}Co, ^{133}Ba, ^{134}Cs, ^{137}Cs, ^{154}Eu and ^{155}Eu from Bugey 1 stack powder samples (05/23/2006). 51
Table 20 - Cumulative leached fraction of ^{60}Co and ^{137}Cs for SLA2 sleeves (07/18/1997). 52

1 Introduction

This report is the Andra contribution to the Carbowaste WP6 survey. It has been written in collaboration with CEA from a previous literature review [1]. We propose therein a state-of-the-art review of leachibility studies on graphite waste which is mainly based on data from French gas-cooled reactors (G2, Bugey and Saint-Laurent). Indeed, France has become involved in disposal studies quite early but this option requires information on the amount and rates of release of radionuclides in the presence of water. Since the late 80's, leaching studies have thus been conducted and in the recent years such studies have also proved useful for the UNGG[1] reactors planned to be dismantled under water.

In this report, the results obtained from these leaching test campaigns are compiled. We try to assess current knowledge on radionuclides leaching behavior in graphite waste but also to identify moot points and important issues to address in future works. In this perspective, leaching experiments should meet a twofold objective:

- From a qualitative point of view, it is intended to establish a release model for the most important radionuclides for graphite waste management ,
- From a more quantitative point of view, the consolidation of the radionuclide inventory and release rate in graphite waste is mandatory to choose realistic – or at least not too conservative – assumptions for safety analyses.

In the following, the main chemical and physical properties of nuclear graphite are introduced first. Special attention is devoted to the evolution of the graphite microstructure and porosity under irradiation as it may significantly affect radionuclides release. Subsequently, available studies on water penetration into non-irradiated and irradiated graphite are reviewed. Leaching results on Hanford, G2, Bugey and SLA2[2] graphite samples are detailed in the next section. ^{36}Cl and ^{14}C release will be more specifically discussed as these radionuclides are of importance for graphite disposal. Eventually, section 5 draws together the conclusions and ongoing works. This document largely calls upon the EDF WP1 report on the current status of graphite waste in France. The reader is thus referred to this survey for further details on UNGG

[1] UNGG : Natural Uranium Graphite Gas reactor.

[2] SLA2 : Saint Laurent des Eaux A2 reactor (UNGG reactor)

technology and reactors as well as on French selected options for graphite treatment and conditioning.

2 Properties of nuclear graphite and evolution under irradiation

2.1 Structure and manufacturing process

Graphite is a particular crystalline form of carbon [2]. It exists naturally and can also be manufactured from petroleum coke and coal tar pitch. The structure of the monocrystal (Figure 1) is formed of non-compact hexagonal sheets, called graphenes, separated by ca. 0.336 nm all along the direction of their normal line. In each sheet, the carbon atoms are strongly bound by covalent bonds of the sp^2 type in a regular paving of hexagonal honeycomb patterns. Bonds between the sheets are weak (Van der Waals interaction). This explains the cleaving and poor hardness of the material.

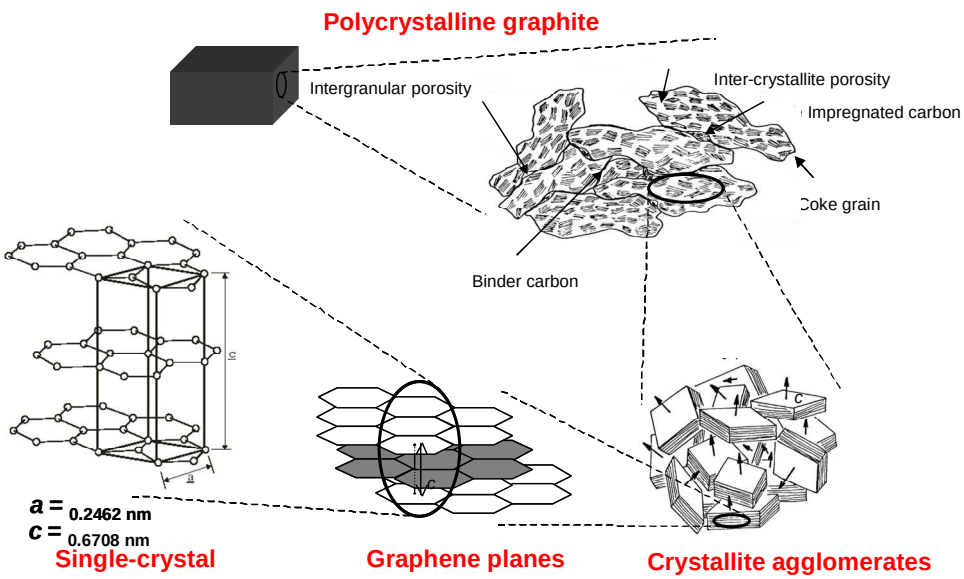

Figure 1 – Structure of graphite [2]

Polycrystalline graphite is used as a structural material in gas-cooled reactors. It is manufactured (Figure 2) from petroleum coke or coal tar pitch plus a binder. The calcined coke is ground and sifted. Resulting grains are then mixed with the binder in appropriate proportions so as to obtain a good density and make the release of volatile materials from the binder easier. The coke blend is generally mixed at 165°C with coal tar pitch, shaped by extrusion or by

either unidirectional or isostatic pressing[3], and then heated between 800°C and 1200°C to coke the binder [3].

The product may then undergo one or more impregnations, generally with petroleum pitch, so as to increase its density and its mechanical properties. Finally, it is graphitized between 2500°C and 3000°C to obtain the hexagonal crystalline structure (Figure 1). Cleaning agents (NaF, MgF_2) are added during graphitization to make graphite of nuclear quality with a low impurity content.

Specific data related to each UNGG reactor - type of petroleum coke and physical characteristics of non-irradiated graphite – can be found in EDF WP1 report.

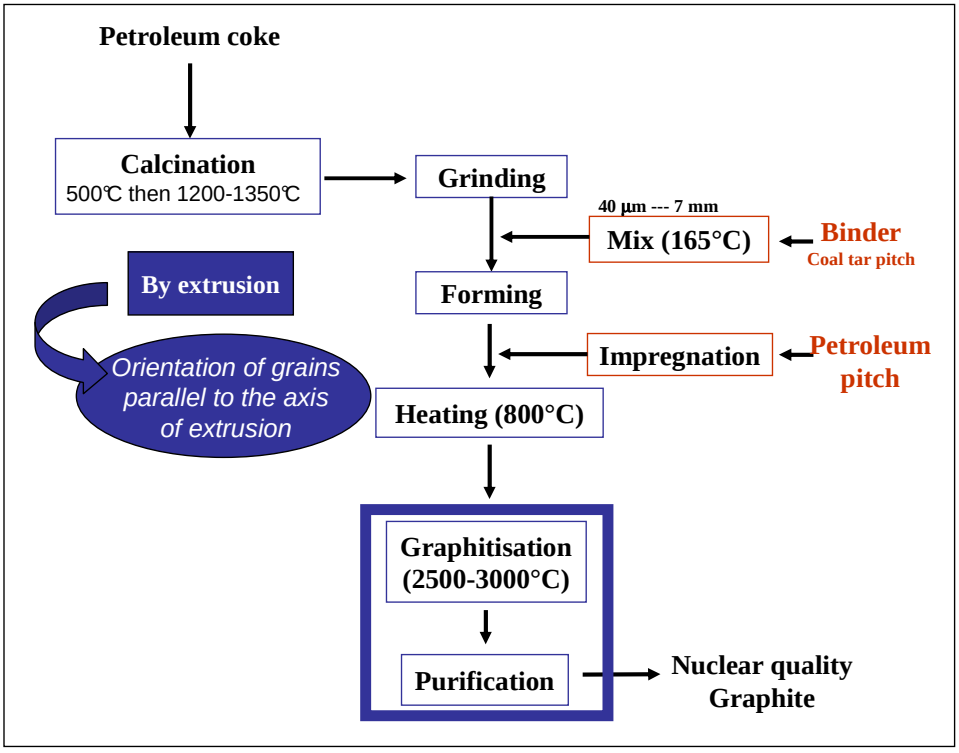

Figure 2 – Nuclear graphite manufacturing process [3].

[3] Isostatic compression means applying an isotropic pressure, that is to say which has the same value in all directions.

2.2 Effects of neutron bombardment

Under neutron radiation, solids undergo physical changes. In graphite moderators, fast neutrons (~ 2 MeV) can displace carbon atoms from the crystal lattice, thus creating interstitial and vacancy defects as shown in Figure 3 [2].

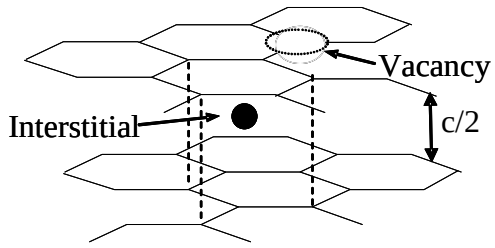

Figure 3 – Defects created during graphite irradiation by fast neutrons [3].

Such defects are responsible for the alteration of the graphite physical properties, *i.e* energy accumulation ("Wigner energy"), mechanical characteristics, geometric dimensions and thermal conductivity.

The creation of defects within the graphite network results in an energy accumulation referred to as "Wigner energy". Wigner energy represents a potential fire risk for air-cooled reactors that operate at low temperature. Indeed, below an irradiation temperature of 120°C, lattice defects are not very mobile so that they lead to a fast build up of energy. When temperature increases, defects become mobile, so Wigner energy can be suddenly released. The amount of releasable energy for an increase of 1°C of 1 g of graphite is referred to as the differential enthalpy, or specific heat. In Figure 4, the differential enthalpy ($dH/d\theta$) is plotted versus graphite temperature for non-irradiated graphite (dashed line) and for graphite irradiated below 120°C (solid line). For irradiated graphite, the differential enthalpy shows a peak at 200°C that exceeds the specific heat of non-irradiated graphite. When irradiated graphite is warmed up, the stored energy starts to be released at the threshold temperature θ_S. When the trigger temperature is reached (θ_D), that is to say when the differential enthalpy exceeds the specific heat of non-irradiated graphite, graphite becomes thermally unstable and its temperature adiabatically rises to θ_f which is determined by the equality of the two shaded areas in Figure 4 [4]. Therefore, a gentle heating of irradiated graphite can lead to an unexpected temperature increase, in turn leading to the destruction of the reactor pile. In order to avoid such an

accident, it is necessary to periodically 'anneal' graphite stacks, which consists in releasing the stored energy in a controlled manner.

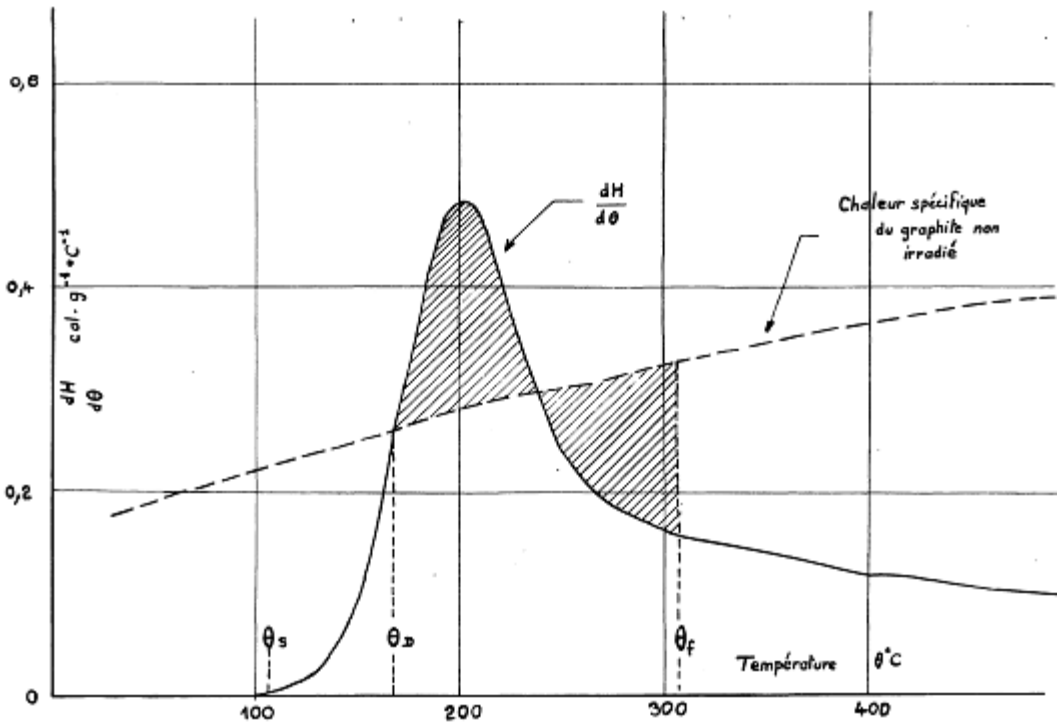

Figure 4 - Wigner energy spectrum of graphite irradiated at 60°C under a neutron fluence of 1.67.10^{20} n.cm^{-2} (or 0.12 displacements per atom) [4].

Theoretically, there is a risk of Wigner effect when [3] the irradiation temperature is lower than 115°C/120°C and the neutron fluence is higher than 1.54.10^{20} n.cm^{-2} (or 0.11 displacement per carbon atom).

In practice, for graphite irradiated between 30°C and 120°C, most of the stored energy is concentrated around the peak at 200°C. The height of this peak decreases as the irradiation temperature increases. When temperature exceeds 170°C, the Wigner energy peak disappears. Indeed, at high temperatures, the irradiation defects do not accumulate anymore because they recombine as soon as they are formed. Beyond 350°C, there is no risk of spontaneous release of Wigner energy.

The mechanical resistance of graphite increases under irradiation. The displacement of atoms, and thus the creation of defects, prevents graphene planes from moving one from another. On the whole, the main graphite mechanical properties (resistance to compression, shearing,

elasticity modulus, hardness) increase with low doses of irradiation. At higher doses, weight loss leads to an increase in porosity and a decrease in mechanical resistance [5].

Under neutron radiation, the creation of vacancies and interstitials makes the unit cell parameter $\vec{c}$ increase and the unit cell parameter $\vec{a}$ slightly decrease [4]. These structural changes depend on the dose, irradiation temperature and physical characteristics of the material (crystallites orientation, porosity, degree of graphitization, thermal expansion coefficient, etc.) [6].

Graphite thermal and electrical properties are also affected. The electrical resistivity of the graphite rapidly increases under irradiation [4] while the graphite thermal conductivity K_0 decreases as the defects created within the crystalline network hinder the propagation of heat waves [5]. In general, the thermal expansion coefficient increases with the radiation dose, but this increase is only significant above 5.10^{20} to 1.10^{21} $n.cm^{-2}$. At low doses, a slight decrease in thermal expansion coefficient values is often observed prior to the increase.

2.3 Graphite oxidation

Under high doses of ionizing radiations, carbon dioxide used as a coolant in UNGG reactors is split into one molecule of CO and one O^{2-} ion. Then, the oxygen ion can react with graphite carbon atoms, and release a gaseous CO molecule. This phenomenon is called wear [2]:

$CO_2 + h\nu \rightarrow CO + O^*$

$O^* + C \rightarrow CO$

It is globally equivalent to the Boudouard reaction [7]:

$CO_2 + C \rightarrow 2\ CO$

Graphite density loss U is due to the radiolytic oxidation and is defined as follows [8]:

$$U(\%) = \left(1 - \frac{d_i}{d_0}\right) \times 100 \qquad (1)$$

where d_i is the apparent density of irradiated graphite and d_o is the density of non-irradiated graphite.

In turn, the oxidation rate is a function of [9] (Table 1):

- the relative volume of the graphite apparent porosity,
- the coolant gas pressure,
- the radiation flux absorbed into CO_2 which characterizes the power of the pile,
- the inverse of the weight of irradiated graphite within the core (specific power) [10]

- the inverse of the absolute temperature of the gas within graphite pores, *i.e* the graphite temperature.

Table 1 - Factors impacting graphite density loss [9].

Reactor[4]	G2	CHA1	CHA2	CHA3-SLA1	Bugey 1
Graphite mass (moderator, tons)	660	800	1300	2000	1500
Pressure CO_2 (bar)	15	25	26.5	26.5	43
Thermal power (MW)	250	300	850	≈ 1600	1920

With the increasing power density of the UNGG reactors, graphite oxidation by CO_2 gas under irradiation becomes important. The oxidation rate, which is already high for CHA1 and SLA1, is even higher for Bugey 1, and it was then essential to use an oxidation inhibitor for this plant [9]. Indeed, Bugey 1 graphite was particularly affected by radiolytic oxidation. At the end of reactor life (12.18 f.p.e.y. , full power equivalent years) the maximum density loss ranged between 25 and 42.5% [11].

Carbon monoxide and hydrogen are average oxidation inhibitors for graphite as they decrease the oxidation rate by a factor of 2 to 4. In contrast, methane, even at low concentrations (500 vpm), reduces the oxidation rate by a factor of 20 [9]. However, whereas methane has a positive effect on graphite oxidation, radiolysis of the $CO_2/CO/CH_4$ mixture forms carboxyhydrogenated deposits in the primary circuit and in particular on graphite surface. The formation of deposits has two origins [7]:

- Methane oxidation is driven by active oxygen atoms (O*). It produces a methane oxidation product (P) which is deposited on the graphite surface:

  $CH_4 + O^* \rightarrow P + CO$

- This methane oxidation product (P) then oxidizes into a compound ('OP') under the action of active oxygen atoms (O*) :

  $P + O^* \rightarrow (OP)_s$

[4] CHA1, CHA2, CHA3 : Chinon A1, A2, A3 reactors – SLA1 : Saint-Laurent des eaux A1 reactor.

- The other source of deposits comes from carbon monoxide radiolysis that produces a carbon suboxide (C_3O_2):

  $4\ CO \rightarrow C_3O_2 + CO_2$
- The carbon suboxide polymerizes at the reactor operating temperature:

  $n\ C_3O_2 \rightarrow (C_3O_2)_n$
- The polymerised carbon suboxide preferentially deposits on the cold parts of the graphite stack as long as the CO content is high enough (CO > 2 to 3%).

Such deposits have a significant influence on the neutron capture cross-section because they are composed of around 1% in weight of hydrogen [12]. The deposits weight in the SLA1 reactor at shutdown in April 1990 has been estimated at 16.6 tons, and that of Bugey 1 at shutdown in May 1994 at 81.6 tons [7]. No measurement of H_2 content in the graphite stacks is available for the other plants (CHA1, CHA2, CHA3 and SLA2). Yet, given the operating conditions of these reactors, the carboxyhydrogenated deposit content must be lower than that of the Bugey 1 reactor.

The production rate of carboxyhydrogenated deposits depends on [7]:

- the graphite temperature
- the methane concentration
- the γ flux and irradiation time

In contrast, CO concentration does not seem to affect the production rate of deposits. Carboxyhydrogenated deposits are situated in the porosity and on the surface of the graphite stacks in all UNGG reactors that have used CO_2 as coolant and in which significant amounts of carbon monoxide were produced by radiolytic oxidation. Using methane as an oxidation inhibitor has increased their formation. The deposits strongly adhere to the irradiated graphite and can only be removed by means of intense mechanical abrasion [7].

2.4 Graphite porosity

2.4.1 Definition of the porosity scale

There are many, often arbitrary, classifications of porosity in relation to the pore size. The cut-off thresholds between the so-called microporous and macroporous domains are different from one author to another and depend on the methods used for investigating the porous medium [13]. It is thus necessary to establish a convention for classifying the various

porous domains. Such a convention has been proposed by Beck [13] who defines porosity intervals (limestone, within the context of his doctoral thesis) as shown in Figure 5:

- *Infraporosity* refers to pores size smaller than 0.01 µm. Flow through infrapores is controlled by adsorption forces,
- *Supraporosity* refers to pores greater than 2,500 µm. Flow is governed by gravitational forces,
- *Capillary porosity* refers to pores between 0.01 and 2,500 µm. Water flow is due to capillary forces. The capillary porosity is divided into three sub-domains referred to as *microporosity*, *mesoporosity* and *macroporosity* (Figure 5).

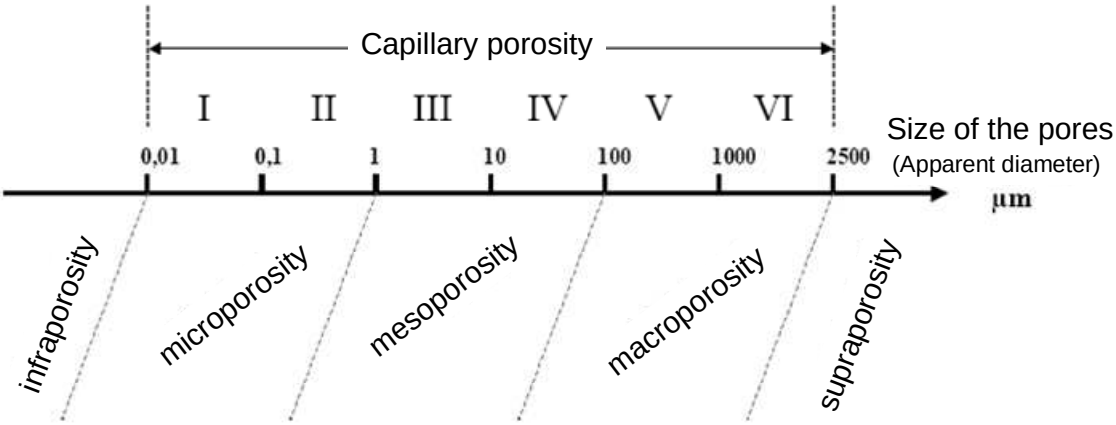

Figure 5 - Porosity class thresholds [13].

2.4.2 Porosity in non-irradiated graphite

The porosity of graphite depends on its manufacturing process [2,14]:

- the nature of the coke and coal tar pitches used,
- the particle size of the grinding coke and the technique used for shaping,
- the creation of cracks by the release of volatile materials during thermal treatments,
- the shrinkage that occurs during the material cooling after graphitization. It produces cracks on the edges of the coke grains as well as in the binder,
- the graphite impregnation. It decreases the graphite porosity, and thus increases its density.

Figure 6 shows the pore size distribution obtained by mercury porosimetry on non irradiated graphite samples from G2 reactor (Lockport L coke).

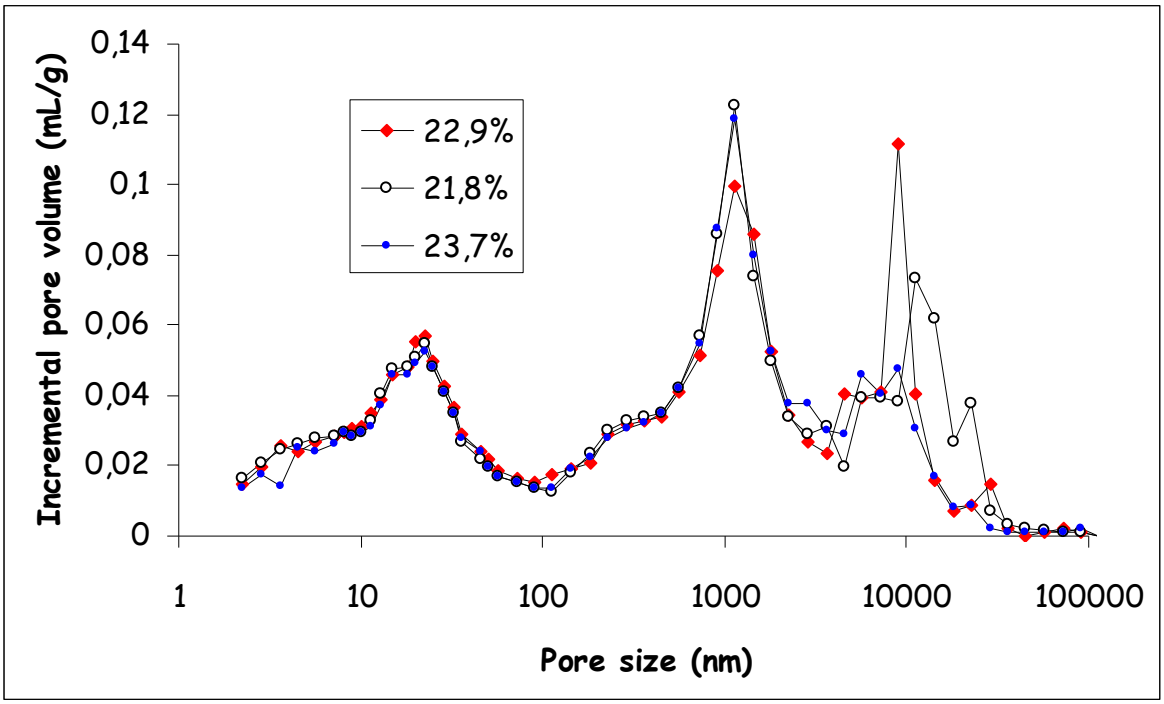

Figure 6 - Distribution of pore diameters for non irradiated graphite (G2 reactor).

Three families of pore size are observed:

- pores smaller than 100 nm whose maximum distribution is located around 20 nm (micropores),
- pores whose size is between 100 nm and 5 µm, with a maximum distribution at 1 µm,
- pores with diameters bigger than 5 µm, with a maximum distribution at 10 µm.

Infraporosity (pore diameter lower than 10 nm) is not accessible using mercury porosimetry. A good reproducibility of the distribution of the pores whose diameter is lower than 5 µm is also observed. The average porosity of the samples is 23%.

2.4.3 Porosity in irradiated graphite

Under irradiation the crystallites swelling alters graphite porosity [15].

In the absence of oxidation (test in helium atmosphere, see Figure 7), neutron radiation makes the graphite specific surface decrease, the relative decrease depending on the dose rate. The pore distribution remains qualitatively unchanged, but the accessible volumes for each pore radius decrease. This may be attributed to the throttling of pores entry because of the crystallite expansion [16,17]. The crystallites swelling is indeed partially absorbed by the porosity.

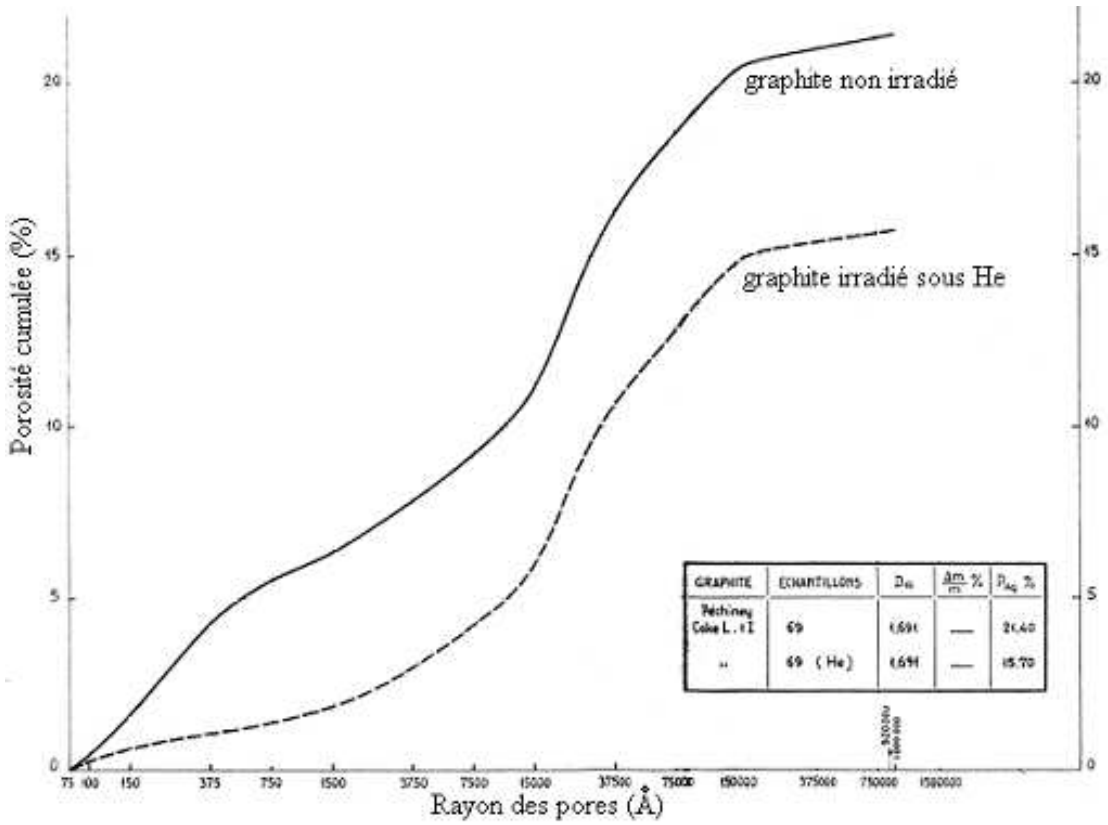

Figure 7 - Variation in porosity as a function of the pore radius for two graphite samples (Lo.L coke): — non irradiated, - - - irradiated under He [18].

Figure 8 shows the evolution of cumulative porosity of graphite with the pore radius under oxidation in CO_2 atmosphere. The crystallites expansion is negligible with the exception of the macroporous domain for which there is an increase in the pore size.

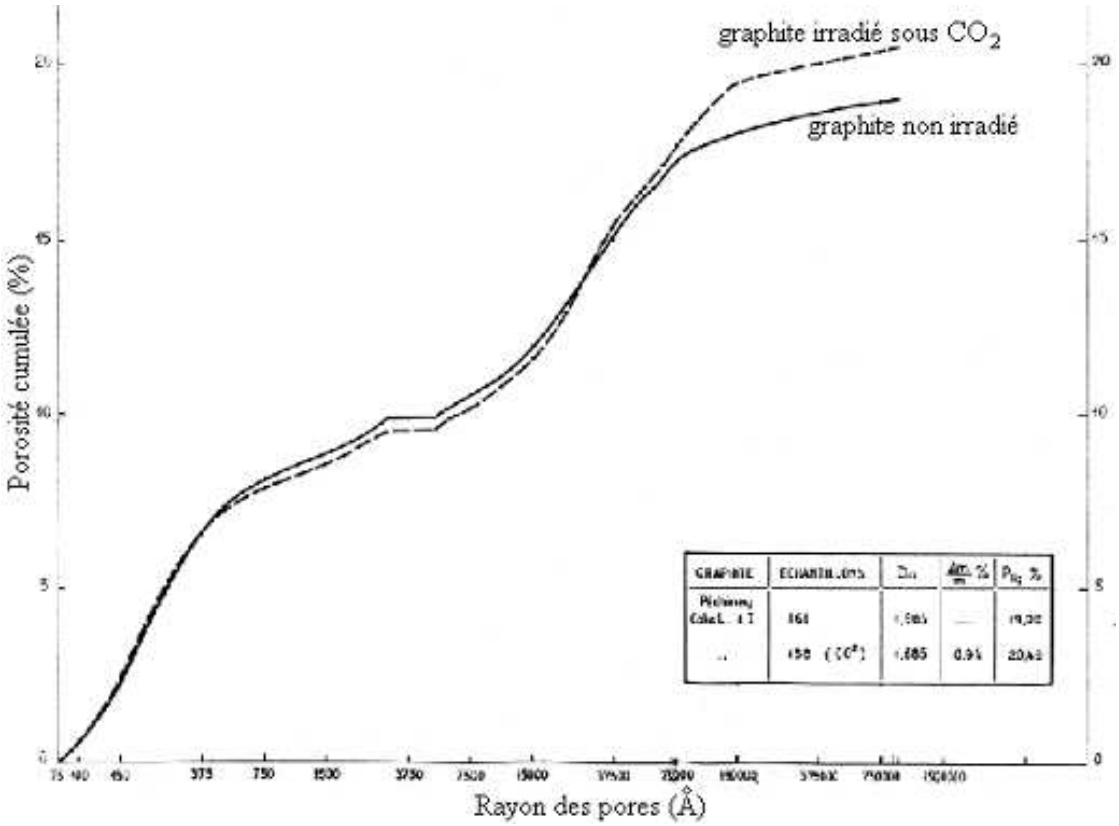

Figure 8 - Variation in porosity as a function of the porous radius for two graphite samples (Lo. L coke): — non irradiated, - - - irradiated under CO_2 [18].

☞ *Summary:*

The graphite porosity depends on the manufacturing process. Under neutron radiation and radiolytic oxidation, porosity is altered. However, available data are often incomplete. It is thus necessary to study the reproducibility of the porosimetry measurements and the evolution of porosity under irradiation.

3 Water penetration into graphite

In this section, results on water penetration into graphite are discussed. It concerns both the amount of water that can come into graphite and the penetration kinetics as these data may influence the radionuclide behavior during leaching tests. Important parameters affecting water penetration are pointed out.

3.1 Water vapor

The interaction between water vapor and graphite is based on a physisorption process [19]. It is reversible between room temperature and 120°C, and becomes significantly irreversible beyond 120°C [20].

The amount of adsorbed water molecules increases with the relative humidity (P/P_s ratio) [21]. At 25°C, it also depends on the sample geometry because of a capillary condensation at the sample edges. The penetration of water and hydrogenated products into graphite increases with the hydration temperature [22].

Nuclear graphite, whatever its density, can adsorb approximately 100 ppm of water from the laboratory atmosphere, and up to 800 ppm when air is saturated with water vapor [8,23]. Most of water molecules are physisorbed but a large part becomes chemisorbed under heating.

3.2 Immersion tests

Areva has studied water penetration into graphite fuel sleeves samples retrieved from SLA (Saint Laurent des eaux) that were initially stored in a disposal pool during decladding. Immersion tests in water were carried out for 24 hours and comparison was made with non irradiated samples. Tests were also performed under pressure to model a 10-meter water column. The mass increase percentages are shown in Table 2.

Table 2 - Percentage of mass increase in irradiated and non irradiated graphite samples [23].

	Irradiated sample (%)	Non irradiated sample (%)
AtmP	4.4	1.1
AtmP + 1 bar	3.8	2.5

On the whole, the water penetration remains small for both irradiated and non-irradiated samples, below 5% in mass. The effect of pressure is also negligible. Yet, the irradiated graphite retains more water than the non-irradiated sample.

Other immersion tests were carried out on non-irradiated graphite from SLA reactors. Both solid samples (whole sleeves) and fragments of various sizes were studied. Their characteristics are shown in Table 3. These samples were immersed in water at room temperature for three months. Regularly, they were drained off (5 minutes) and weighed.

Table 3 - Characteristics of graphite samples used in the immersion tests.

N°	Origin	Dimensions		Mass (g)	Density
		ϕ (in/out) (mm)	Height (mm)		
Fuel sleeves 1	Péchiney	93/136	460	6489.2	1.824
Fuel sleeves 2	SLA	111/137	603	5245.1	1.696
Fuel sleeves 3	SLA	Fragments: > 50, 33-50, 10-33, 4-10, 1-4		-	1.696

The water adsorption rate T_a is defined in (2) and its evolution is plotted in Figure 9.

$$T_a = \frac{m_e}{m_i} = \frac{m_h - m_i}{m_i} \qquad (2)$$

m_i: initial mass of dry graphite,

m_h: mass of the wet sample after wetting and draining,

m_e: mass of the water retained in graphite (core + surface)

T_a: water adsorption rate after draining.

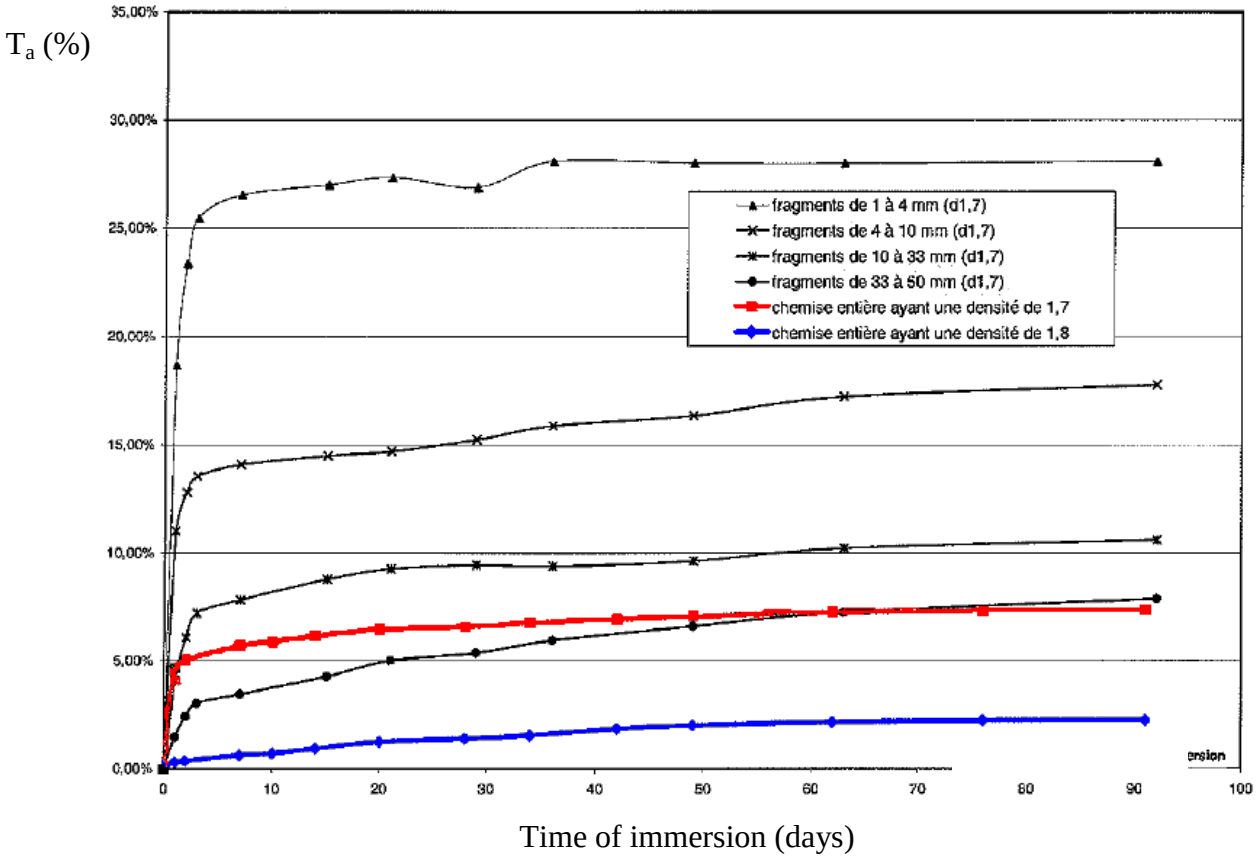

Figure 9 – Evolution of the water adsorption rate of non irradiated graphite with time.

From Figure 9 there is evidence that the water adsorption rate depends on the sample density as well as on the dimensions of graphite pieces:

- The less dense (and more porous) the graphite, the higher the water adsorption rate
- The larger the specific exchange surface, the higher the water adsorption rate (surface wetting).

The water adsorption rate is also temperature-sensitive: the water adsorption kinetics considerably increases when graphite is immersed in boiling water.

Water adsorption measurements were also undertaken on non-irradiated graphite from the Fort St Vrain reactor (USA). Tests were performed in a leakproof container filled with water, either under atmospheric pressure or under 4 bar of nitrogen gas. After 76 days at atmospheric

pressure, the mass increase of the graphite samples was around 1.1% whereas the water mass increase was around 9% after 7 days under 4 bar of nitrogen gas.

☞ Summary:

There may be two mechanisms of water penetration into graphite:

- a physisorption process that occurs as soon as graphite comes into contact with humid air,
- a water retention process that seems to depend on the contact surface and on the graphite porosity. Experiments show that water adsorption kinetics is also temperature and pressure-sensitive.

Few data is available for irradiated graphite. Yet, irradiation can strongly influence water penetration because it alters graphite porosity and it can form carbohydrogenated layers. Further studies are thus required.

4 Leaching behavior of graphite radionuclides

This section aims at reviewing all the leaching experiments on UNGG irradiated graphite available in the literature. First, experimental leaching protocols will be presented. Then results will be discussed for each radionuclide.

4.1 Description of studies

Most of leaching studies were carried out by the CEA on graphite from either EDF plants (Bugey and Saint-Laurent SLA2) or CEA G2 reactor. Leaching tests were also performed by the Pacific Northwest Laboratory (PNL) on irradiated graphite from the CEA G2 reactor and the American Hanford reactor. Details on French UNGG reactors can be found in the EDF WP1 report.

Experimental conditions are collected in Table 4 and are divided into three sections: graphite origin, sample dimensions and leaching conditions.

It is of importance to note that experimental conditions, in particular sample dimensions (V/S ratio), leachate volume and renewal, are significantly different. This is a serious limitation since it precludes reliable comparisons, and therefore no clear conclusion on radionuclide behavior can be drawn. Moreover, when such leaching test campaigns were undertaken, underwater dismantling was not relevant yet. Therefore, experiments were often conducted with two compositions of the leaching solution:

- ultrapure water (used as a reference)
- lime water (representative of disposal in concrete packages).

The first leaching tests were carried out at the PNL laboratory in 1988 and 1989 on irradiated graphite samples from **Hanford** [24] and **G2** [25] reactors. The release of ^{36}Cl and ^{14}C was followed for 8 to 13 weeks. Leaching tests were conducted in pure water and in simulated groundwater from 20 to 90°C. Prior to leaching, graphite samples were cleaned by immersing them in 200 to 300 mL of demineralized water in an ultrasonic bath for 1 to 2 minutes to remove manufacturing dust. They were then completely immersed in leakproof containers and saturated with air to prevent isotopic exchange between ^{14}C and the CO_2 present in air. The entire leachate volume was analyzed every week. This experimental protocol is in agreement with ANSI/ANS.16.1.1986 standards.

Table 4 - Leaching conditions for graphite samples from Hanford, G2, SLA2 and Bugey1 reactors.

Origin		Hanford	G2	Hanford	G2	SLA2	Bugey	Bugey	G2
Component		Moderator				Sleeve	Moderator		
Lab		**PNL**		**CEA**					
Sample dimensions	Size (mm)	D = 30 H = 30		D = 80 H = 80	D=H=80 or D=H=33	D = 19 H = 13	D = 16 H = 33	powder	D = 64 H = 18 or 15
	V/S (cm)	0.5		1.26	1.26 or 0.55	0.27	0.33	-	0.58 or 0.51
	m (g)	~ 40		~ 650	~ 650 or 50	~ 6	~ 10	~ 1.5	~ 90 or 75
	S_{spe} or ε	5.2 m²/g	0.27 m²/g	ND			~23%	ND	23%
Leaching conditions	Leaching duration (days)	56	91	90		455	144 or 455	184	454
	Medium	UP water groundwater	UP water			Industrial water*	UP water and lime water	UP water	UP water and lime water
	Renewal	Complete for each analysis					Partial	Complete for each analysis	
	T (°C)	20, 50 and 90	20	23		20	20 and 40	20	20
	V_L (mL)	406		3000	3000 or 500	150	20	10	150
	V_L/S (cm)	9,27		~ 10		11.9	1	-	1.5 or 1.6
	RN monitored	^{36}Cl, ^{14}C		^{36}Cl, ^{14}C, ^{3}H, ^{60}Co, ^{137}Cs , ^{63}Ni		^{36}Cl, ^{14}C, ^{3}H, ^{60}Co, ^{137}Cs	^{36}Cl, ^{14}C, ^{3}H, ^{60}Co, ^{137}Cs, ^{63}Ni	^{36}Cl, ^{14}C, ^{3}H, ^{60}Co, ^{137}Cs, ^{134}Cs, ^{133}Ba, ^{154}Eu, ^{155}Eu	^{36}Cl, ^{14}C, ^{3}H, ^{60}Co, ^{137}Cs, ^{63}Ni, ^{133}Ba

V_L: leachate volume, S: sample surface in contact with the liquid, V: sample volume, m: graphite mass, T: leachate temperature, S_{spe}: specific surface of the graphite, ε: porosity of the graphite, RN: radionuclide, D: diameter, H: height

*Industrial water: Ca^{2+} = 78 mg/L, Mg^{2+} = 24 mg/L, Na^{+} = 5 mg/L, K^{+} = 1 mg/L, SO_4^{2-} = 10 mg/L, HCO^{3-} = 357 mg/L, Cl^{-} = 4,5 mg/L, NO^{3-} = 3,8 mg/L, pH = 7,2

A comparative study was carried out by the CEA on the same samples (G2 and Hanford reactors) as the PNL leaching studies [26]. G2 samples came from both the reflector (core n°2) and the moderator (cores n°13 and 14). The experimental procedure respects the guidelines of the standard BECC-FT 04.020 test. Samples were immersed in pure water, in closed but not leakproof containers. Sample dimensions were quite different from that of PNL tests - 650 g for the CEA *vs.* 40 g for the PNL – preventing any reliable comparison.

Complementary tests on G2 irradiated graphite samples were thus undertaken in 1990. They dealt with smaller graphite samples (50 g) taken from the same coring than previous tests (cores n°12 and 15) in order to be comparable with PNL results. The experimental procedure was also modified accordingly by using a leakproof container saturated with air.

In 1999, leaching tests were also carried out by the CEA [27,28] on three graphite samples from the **Saint-Laurent A2 (SLA2) sleeves,** with different dose rates. The reactors were specially designed to achieve containment. Tests were performed according to the ANDRA 330 ET 09.06 engineering test.

Leaching data are also available for Bugey 1 graphite stack [29]. Cores were taken from various channels and heights within the stack to be representative of different irradiation and temperature conditions. Experiments were conducted in accordance with the ANDRA engineering test, with some modifications however:

- Leakproof design,
- Sampling of the solution under argon sweeping,
- Partial renewal of the leachate for each sampling to increase chlorine concentration,
- Limitation of the V_L/S ratio to 1 cm to increase activity (V_L is the leachate volume and S is the sample geometrical surface).

Three leaching series were conducted using either pure water or lime-saturated water at 20°C or 40°C.

In 2006, similar leaching tests were performed on graphite dust coming from the previous Bugey1 measurement campaign [30]. Powder samples were grinded manually to obtain the finest particle size (< 200µm).

The last study was performed in 2004 on graphite from G2 reactor [31]. Samples were taken from core n°36 which comes from the 1989 coring campaign. A graphite block

corresponding to the total height of the stack (9.4 m) was cut vertically in the radial plane and split into 47 cores that were 20 cm high. The test was made in a leakproof container using argon as an inert gas.

In the following, results are detailed for each radionuclide, with a focus on ^{36}Cl and ^{14}C that are the most problematic isotopes for waste treatment and disposal. We try each time to point out salient features of radionuclide behavior as well as uncertainties and questionable results. This will also allow determining the optimum conditions for conducting leaching experiments.
As already stated, most of the experiments reported last for a minimum duration of 90 days. Thus, in order to make comparisons easier, results will be defined in terms of the cumulative leached activity *F* over 90 days:

$$F(\%) = \frac{\sum_{i=0}^{90} a_i}{A_0} \times 100 \qquad (3)$$

We also mention the so-called EL_{90} which is independent of the sample dimensions:

$$EL_{90}(\mu m) = \frac{\sum_{i=0}^{90} a_i}{A_0} \times \frac{V}{S}(cm) \times 10^4 \qquad (4)$$

where V/S is the sample volume/geometrical surface ratio, A0 is the initial activity and ai the released activity over the leaching time.

4.2 Behavior of ^{36}Cl

4.2.1 Leaching of graphite from G2 and Hanford reactors

4.2.1.1 Results from the PNL laboratory

Results of PNL leaching tests are presented in Table 5, after 90 days of leaching for G2 samples and 56 days for Hanford samples [24,25]. As G2 and Hanford graphite moderators are of different nature and have different operating history, comparisons are not straightforward. For the Hanford reactor, the cumulative leached fraction of ^{36}Cl after 56 days seems to be independent of the leaching conditions. Results are comparable whatever the temperature (25, 50 or 90°C) and the nature of the solution (pure water *vs.* groundwater).

Table 5 - Cumulative leached activity of ^{36}Cl for G2 (1988) and Hanford (1987) reactors (PNL results).

Reactor	N°	Medium, T (°C)	V_L/S (cm)	V/S (cm)	Graphite mass (g)	A_0 (Bq/g)	F (%)	EL_{90} (µm)
Hanford (PNL)	DIW25	Water, 25°C	9.25	0.5	40	2500	0.20*	10*
	DIW50	Water, 50°C					0.20*	10*
	DIW90	Water, 90°C					0.19*	10*
	HGW25	Groundwater, 25°C					0.16*	8*
	HGW90	Groundwater, 90°C					0.17*	8*
G2 (PNL)	2	Water, 20°C				940	3.7	185
	13					4460	39.1	1955
	14					4480	0.96	48

* at 56 days

For G2 reactor, results are much more variable. The ^{36}Cl release ranges from 1 to 40% of the initial activity. Surprisingly enough, whereas cores n°13 and 14 have similar properties (initial activity and thermal history), their cumulative leached fraction is different. Gray and Morgan have tried to explain such a difference [24,25]. They propose that chlorine 36 release may be either limited by:

- Diffusion of reagent (such as O_2) or products within graphite pores,
- Depletion of the chlorine 36 content.

Yet, Figure 10 shows that diffusion is not rate-determining because the cumulative leached fraction F should be proportional to the square root of time otherwise. Depletion of chlorine 36 content is also unlikely because released fractions are low. It is possible however that part of chlorine atoms is more reactive or more accessible to leachate.

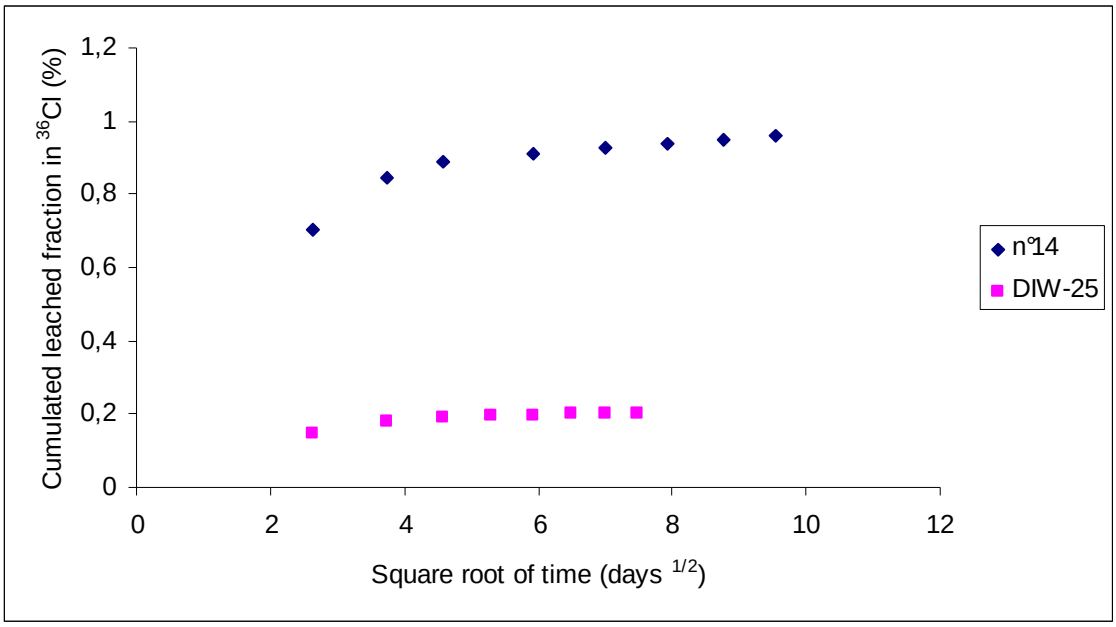

Figure 10 - Cumulative leached fraction of ^{36}Cl as a function of square root of time for G2 (core No.14) and Hanford (DIW-25) graphite samples (pure water, room temperature).

4.2.1.2 Results from the CEA

Results are presented in Table 6 after 90 days of leaching.

Table 6 - Cumulative leached fraction of ^{36}Cl for G2 (09/01/1988) and Hanford (06/24/1989) reactors (CEA results).

Reactor	N°	Medium, T(°C)	V_L/S (cm)	V/S (cm)	Graphite mass (g)	A_0 (Bq/g)	F (%)	EL_{90} (µm)
Hanford (CEA)	D1	Water, 23°C	10	1.26	650	1670	0.30	38
	E2					1490	0.28	35
	G3					1700	0.32	41
G2 (CEA)	2					400	0.34	43
	13					1275	1.74	219
	14					530	1.05	132

Results for Hanford graphite are similar to that obtained by PNL (low ^{36}Cl release), with a mean cumulative leached fraction of 0.30%.

For G2 samples, cores 13 and 14 release the same amount of chlorine 36 whereas core n°2 shows a lower cumulative leached fraction. This is in line with the origin of graphite samples,

as core n°2 comes from G2 reflector while cores 13 and 14 were retrieved from G2 moderator. Differences are observed on F values for cores N° 2, 13 and 14 between CEA results (Table 6) and PNL results (Table 5). They may stem from different measurement techniques or protocols. The mass of graphite samples in CEA tests (650g) strongly differs from samples in PNL tests (40g). To check whether the sample mass affects leaching rates, complementary experiments were performed on G2 cores n° 12 and 15. Such cores are located on either side of cores n°13 and 14. Thus they should release similar amounts of chlorine 36. Results are shown in Table 7. Samples dimensions (V/S) and solution volume (V_L/S) were modified according to PNL experimental conditions.

Table 7 - Leaching results for G2 and influence of graphite mass.

Core n°	Medium, T(°C)	V_L/S (cm)	V/S (cm)	Mass (g)	A_0 (Bq/g)	F (%)	EL_{90} (µm)
2	Water, 23°C	10	1.26	650	400	0.34	43
13					1275	1.74	219
14					530	1.05	132
12			0.55	50	654	20.2	1111
15					920	53	2915

Two important conclusions can be drawn from Table 7:

- First, leaching rates largely depend on graphite samples dimensions (mass and V/S ratio). F values are 20 to 50 times higher for small samples than for bigger ones. This is in agreement with the diffusion of chlorine 36 through graphite porosity: the larger the size of the graphite sample, the slower the release kinetics.
- Then, whereas PNL and CEA experiments are conducted under similar conditions, release rates are different (see Table 5 and Table 7). No explanation has been proposed, and we do not understand such a result either.

☞ *Summary:*

This first study shows the strong influence of the sample dimensions (mass and V/S ratio) on ^{36}Cl leaching rate. This behavior should be correlated with the accessibility of graphite pores to the leaching solution.

4.2.2 Other graphite leaching tests on G2 stack

The most recent leaching study was performed in 2004 on G2 graphite. Core n°36 was cut into several slices 15 or 18 mm thick to make samples of c. 75 or 92 g [31]. Under operating conditions such samples were subjected to a temperature in the order of 300°C. Leaching tests were conducted in ultrapure (UP) water or in lime water at 20°C for 455 days. Results are shown in Table 8 (for 97 days of leaching) and Figure 11 (for 455 days of leaching).

Table 8 - Cumulative leached fraction of ^{36}Cl for G2 stack graphite (03/09/2004).

Reactor	N°	Medium, T(°C)	V_L/S (cm)	V/S (cm)	A_0 (Bq/g)	F (%)	EL_{90} (µm)
G2 Core n°36	2	UP water, 20	1.5	0.58	216	82	4723
	6		1.6	0.51	254	82	4190
	9		1.5	0.58	394	89	5126
	5	Lime water, 20	1.6	0.51	283	83	4241
	8		1.5	0.58	353	83	4781
	10		1.5	0.58	307	88.8	5115

Chlorine released fractions are high, above 80% for all samples, and they do not seem to depend on the leaching medium (lime water *vs.* ultrapure water). The release process is rapid, as displayed in Figure 11: more than 80% of the initial activity is leached in the first month, and the residual fraction is then released much more slowly.

The presence of two “forms” of chlorine 36 has been proposed to explain release kinetics [31]:

- The major fraction - around 80% - may be weakly bound to graphite and/or located in the graphite macroporosity,
- The complementary fraction may be strongly bound to graphite (covalent bonds) and/or located in the graphite infraporosity.

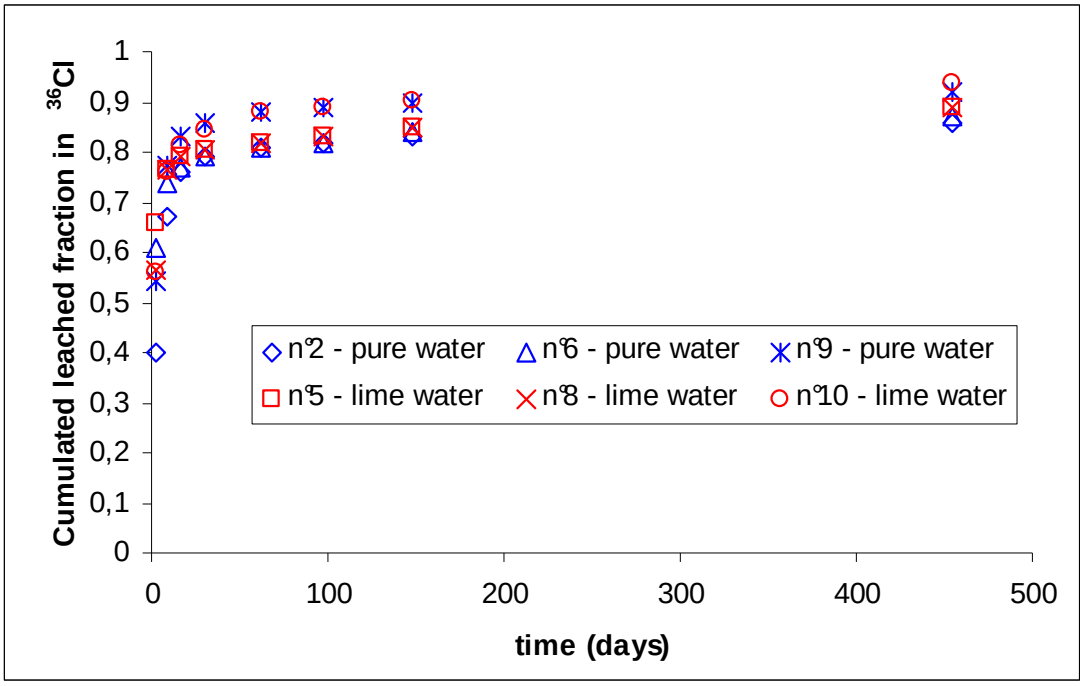

Figure 11 - Evolution of the cumulative leached fraction of ^{36}Cl with time (G2 reactor).

☞ *Summary:*

This last study on G2 graphite has shown a good repeatability of the experiments within a single core. It suggests that the graphite structure is relatively homogenous within the same core and that water penetration is similar for all samples. Moreover, the chemical composition of the aqueous solution does not have any influence on the chlorine 36 leaching behavior.

As a result, chlorine 36 release may be controlled by one of the following processes:

- Water penetration into graphite,
- Chlorine solubilization in the leaching solution, limited either by the nature of chemical bonding between chlorine atoms and graphite or by the location within graphite porosity,
- Transport of chlorine through graphite pores, from the chlorine site to the solution.

The rate-determining step (the slowest process) will determine the kinetics of chlorine 36 release into solution.

4.2.3 Graphite leaching of Bugey 1 stack

Leaching results for Bugey 1 stack samples are shown in Table 9 after 144 or 455 days of leaching [29,30]. Both solid and powder samples were used. The leachate was partially renewed.

Table 9 - Cumulative leached fraction of ^{36}Cl for Bugey 1 graphite stack for solid (09/17/2001) and powder (05/23/2006) samples.

Reactor	N°	Channel	Position (m)	Dose rate (µGy/h)	Medium, T(°C)	V_L/S (cm)	V/S (cm)	A_0 (Bq/g)	F (%)
Bugey (blocks)	N55	D6J4	12	12	Water, 20°C	1	0.33	22	83.5
	N58	D6J4	20.4	8				3.6	38.2
	N75	D6J4	12	20				65	87.5
	N76	D6J4	13.7	40	Water, 40°C			161	83.5*
	N85	D1J1	12	32				82	73.5*
	N86	D1J1	13.7	40				104	36.1*
	N57	B8J0	17.3	80	Lime water, 20°C			16	18.1
	N59	B8J0	21.4	14				18	<3.8
	N98	C6J0	20.4	70				3.6	<18.1
Bugey (powder)	N87	B8J0	17.3	-	Water, 20°C	-	-	10	51
	N67+N68	B3I9	20.4	-				340	1.5
	N88	B8J0	20.4	-				18	14.5

* values after 144 days of leaching

4.2.3.1 Block samples

Figure 12 shows the cumulative released fraction of ^{36}Cl as a function of time. On the whole, there is a large variability on the results as released fractions range from 10% to 90%. However, as for G2 samples, all plots feature a similar pattern, with a fast release of chlorine 36 in the first two months while release remains almost constant beyond two months.

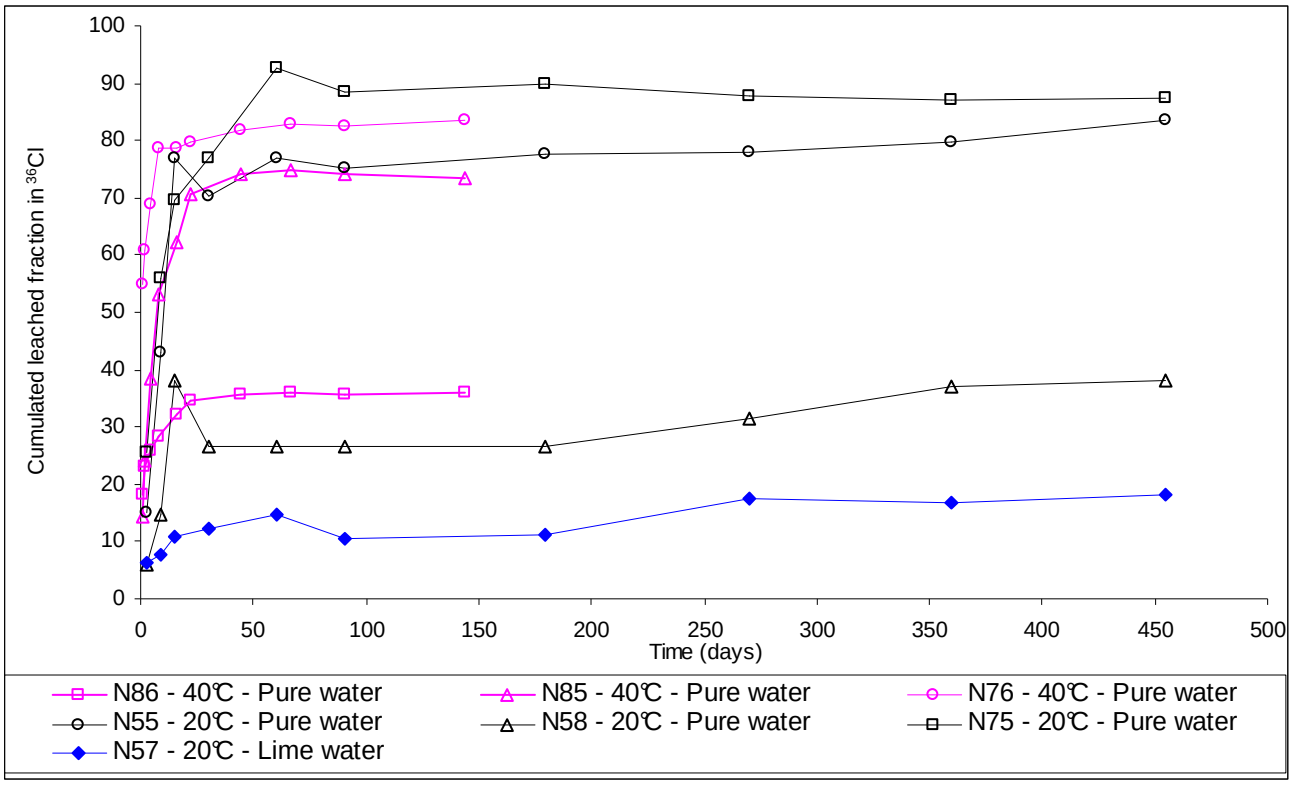

Figure 12 - Impact of experimental leaching conditions on the evolution of the cumulative released fraction of ^{36}Cl (09/17/2001) with time [29].

The effect of the leachate temperature is not significant so bonds between chlorine atoms and graphite should not be temperature-sensitive below 40°C. In contrast, the ^{36}Cl release kinetics is reduced by a factor of 2 to 10 in the presence of lime water [29]. In such a case, the cumulative leached fraction of ^{36}Cl is constant with the square root of time, which suggests a diffusion-driven release mechanism. Several explanations have been discussed to explain the reduction of ^{36}Cl release kinetics in lime water:

- Precipitation of chlorine atoms in the presence of lime water. Yet, this is unlikely because $CaCl_2$ is highly soluble,
- Precipitation of lime or calcite could block off the graphite superficial porosity, thus slowing down ^{36}Cl diffusion [29]. However, tests on G2 graphite did not reveal any difference between results in pure water and those in lime water [31].

As mentioned in Table 9, samples were retrieved from various channels and heights in the stack. Therefore, differences between chlorine 36 cumulative leached fractions in pure water

and in lime water could be explained by the position in the reactor and not by the nature of the leaching solution.

In Figure 13, the cumulative released fraction of ^{36}Cl is plotted as a function of the initial activity of ^{36}Cl, but no correlation is observed.

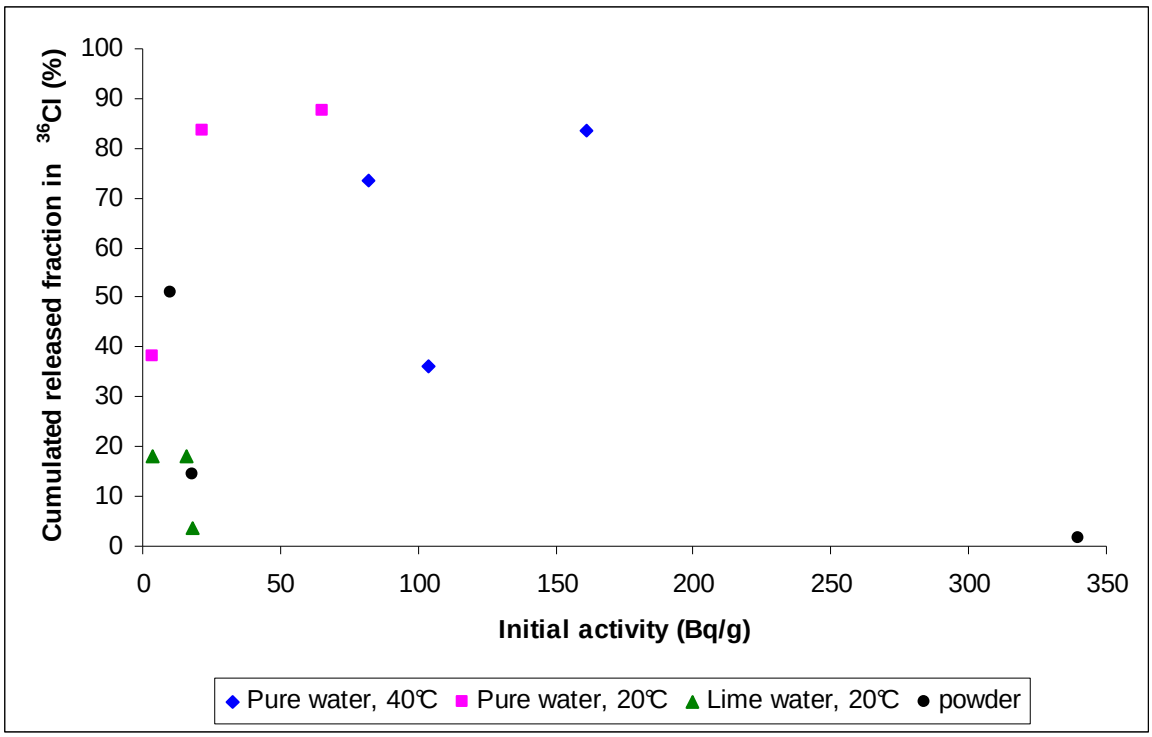

Figure 13 - Cumulative released fraction of ^{36}Cl versus the initial activity in the sample (blocks and powder, from Table 9).

On the contrary, in Figure 14, there is a clear dependency between the height of the graphite sample within the stack and the cumulative released fraction of ^{36}Cl: the deeper the graphite sample, the lower the ^{36}Cl release.

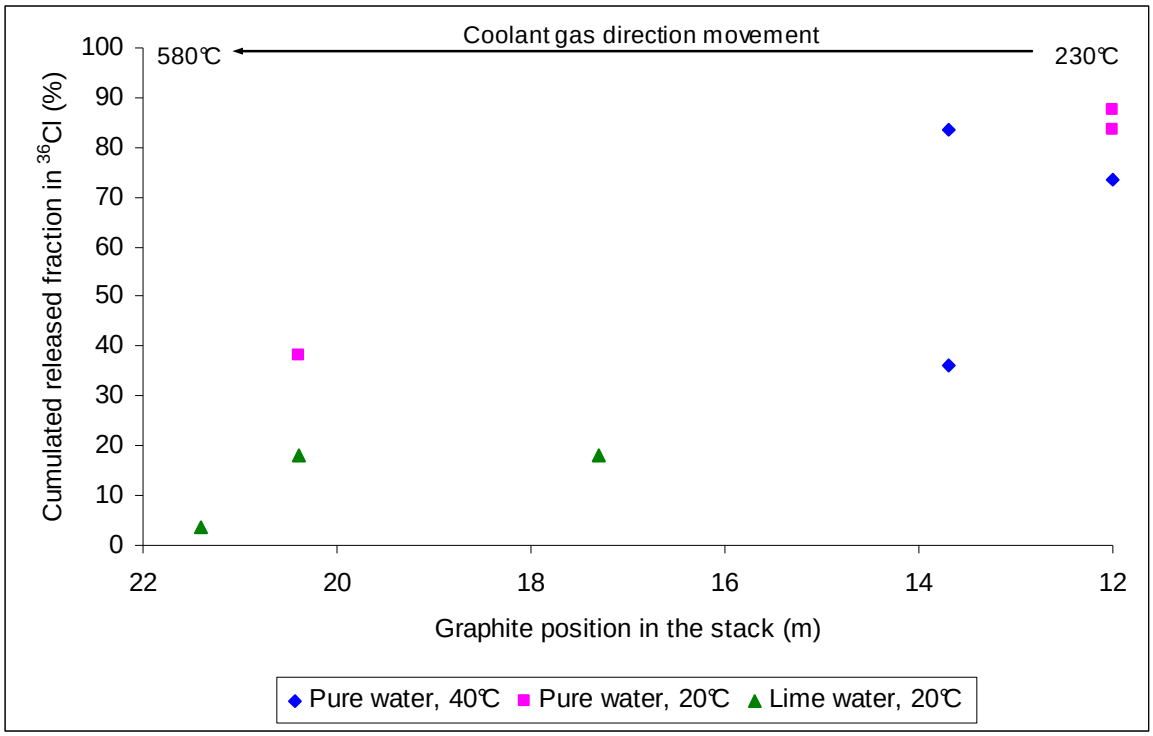

Figure 14 - Cumulative leach fraction of ^{36}Cl as a function of the position of graphite samples in the stack.

The position in the stack is related to the graphite temperature during the operating time, which has in turn a strong influence on the formation of carboxyhydrogenated deposits. In Bugey 1, temperature ranged from 230°C in the upper part of the reactor to 580°C at the bottom. It can be assumed that deposits were preferentially formed where the temperature is high, that is to say where the ^{36}Cl release is low. Then, deposits formed in the graphite porosity and on the surface could prevent or at least slow down the chlorine release into solution.

It would be interesting to carry out complementary experiments on graphite from different heights in the stack in UP water at 20°C so as to confirm the effect of the thermal history of graphite on chlorine 36 release.

4.2.3.2 Powder samples

Powder samples come from radiochemical measurements performed in 1999. Experiments were conducted in UP water at 20°C. Figure 15 shows the cumulative released fraction of ^{36}Cl after a leaching period of 184 days as well as data from previous tests on block samples (see Figure 14).

On the whole, leaching data on powder samples confirm that the chlorine 36 release into solution is correlated with the operating history of graphite (temperature, radiolytic oxidation, deposits), and decreases as the operating temperature increases. We also observe (not shown in Figure 15) that almost all of the chlorine 36 content in the powder is released within the first month which may be explained by high specific surface of powder samples.

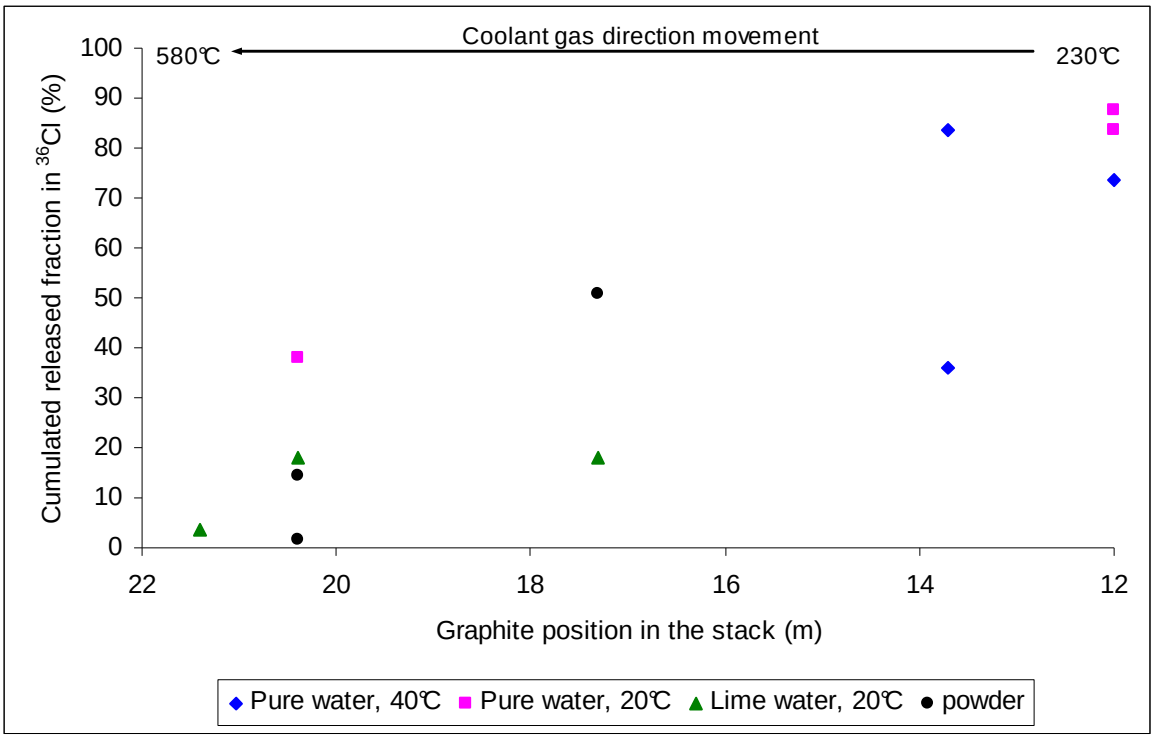

Figure 15 - Fraction of ^{36}Cl released into solution as a function of the position of graphite in the stack for solid and powder samples.

☞ *Summary:*

Studies on Bugey 1 graphite stacks confirm that there is no correlation between the initial chlorine 36 activity and the cumulative leached fraction. There is no relation between the initial activity of chlorine 36 and the position of graphite in the stack either.

The fraction of ^{36}Cl released in solution ranges from 10 to 90%. Such a difference is attributed to the position of graphite samples in the stack, and thus to their thermal history.

As for G2 graphite samples, release seems to occur in two steps, suggesting the presence of two forms of chlorine 36.

4.2.4 Graphite leaching from sleeves in Saint-Laurent A2

Leaching results for SLA2 fuel sleeves are presented in Table 10 after 90 days of leaching [27,28].

Table 10 - ^{36}Cl cumulative leached fraction for graphite samples from SLA2 sleeves (07/18/1997).

Reactor	N°	Medium, T(°C)	V_L/S (cm)	V/S (cm)	Dose rate (µGy/h)	A_0 (Bq/g)	F (%)	EL_{90} (µm)
SLA	01	Water, 20	11.9	0.27	30	76	10	270
	07				120	483	5.6	151
	24				12	70	<5.5	<149

The cumulative released fractions of chlorine 36 are similar for samples n° 01 (10%) and 07 (5.6%), but below the detection limit for sample n°24. As for Bugey samples, there is no clear correlation between initial activities and cumulative released fractions. For instance, sample n°07 has the highest initial activity (483 Bq/g) but its cumulative released fraction is lower than that of sample n°01 whose initial activity is only 76 Bq/g. There is no correlation between the irradiation (dose rate) of graphite and the released fraction either.

As observed in Figure 16, the cumulative released fraction in samples n°01 and 07 is proportional to the square root of time which is characteristic of a diffusion process. Sample n°24 is not displayed because the chlorine 36 activity is below the detection limit.

It is interesting to note that the ^{36}Cl cumulative released fraction for SLA2 sleeves is quite different from that previously observed on graphite stacks (G2 and Bugey reactors): the released fraction is significantly lower and seems to occur progressively, in contrast to the two-step process mentioned for G2 and Bugey 1 stacks. Indeed, the SLA2 graphite sleeves were probably decladded under water so leaching results in Figure 16 could represent the end of the leaching curve (second step) observed for G2 and Bugey graphite samples (see Figure 11and Figure 12). Moreover, graphite sleeves underwent a double impregnation during the manufacturing process, resulting in a lower porosity. This could also slow down the ^{36}Cl release.

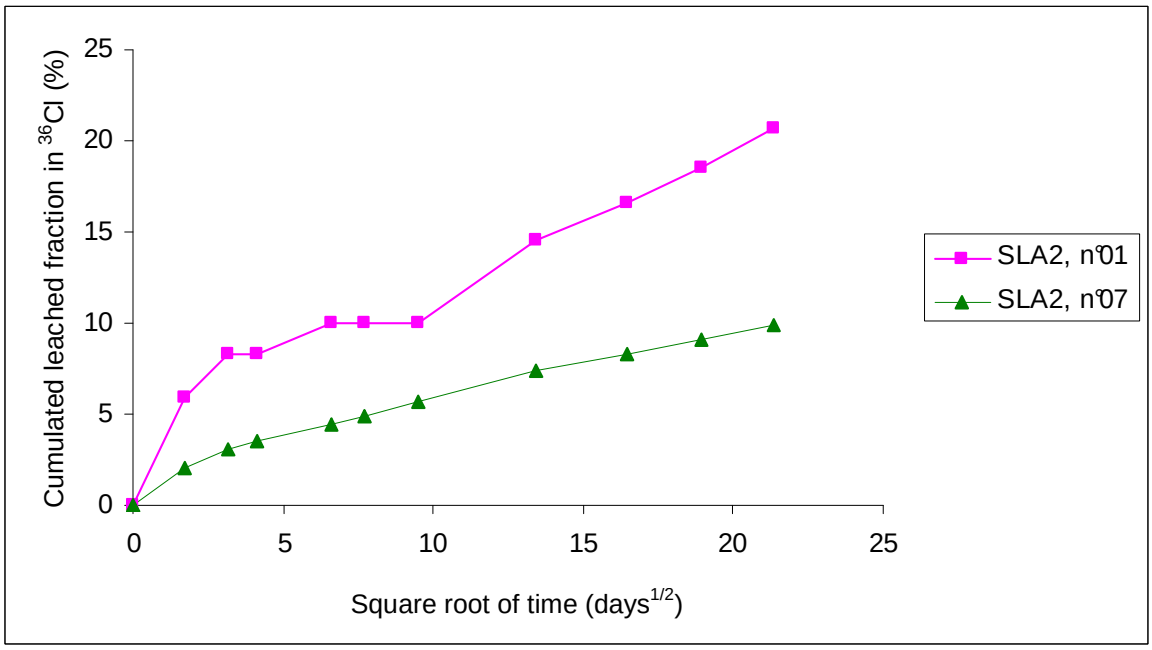

Figure 16 - ^{36}Cl cumulative leached fraction versus the square root of time for two SLA2 sleeves samples.

4.2.5 Diffusion measurements of ^{36}Cl in G2 and Bugey 1 graphite

In a first approach, it has been assumed that chlorine 36 leaching is controlled by diffusion though the graphite porosity. Diffusion calculations were thus made and diffusion coefficients were fitted in order to reproduce the experimental data according to the following equation:

$$F = 2 \times \frac{S}{V} \times \sqrt{\frac{D_a \times t}{\pi}} \qquad (5)$$

where F is the leached fraction, S is the geometrical surface subjected to leaching, V is the sample geometrical volume, t is time and D_a stands for the apparent diffusion coefficient.
As suggested by leaching tests on G2 and Bugey samples, two forms of chlorine 36 were considered:

- a labile fraction of ^{36}Cl (80%), called site 1
- a complementary fraction (20%) of ^{36}Cl, called site 2, that diffuses more slowly. It may be located in the graphite infraporosity and thus it may be less accessible to water.

Figure 17 shows the evolution in the leached chlorine 36 fraction with time, as well as the calculated diffusion profile.

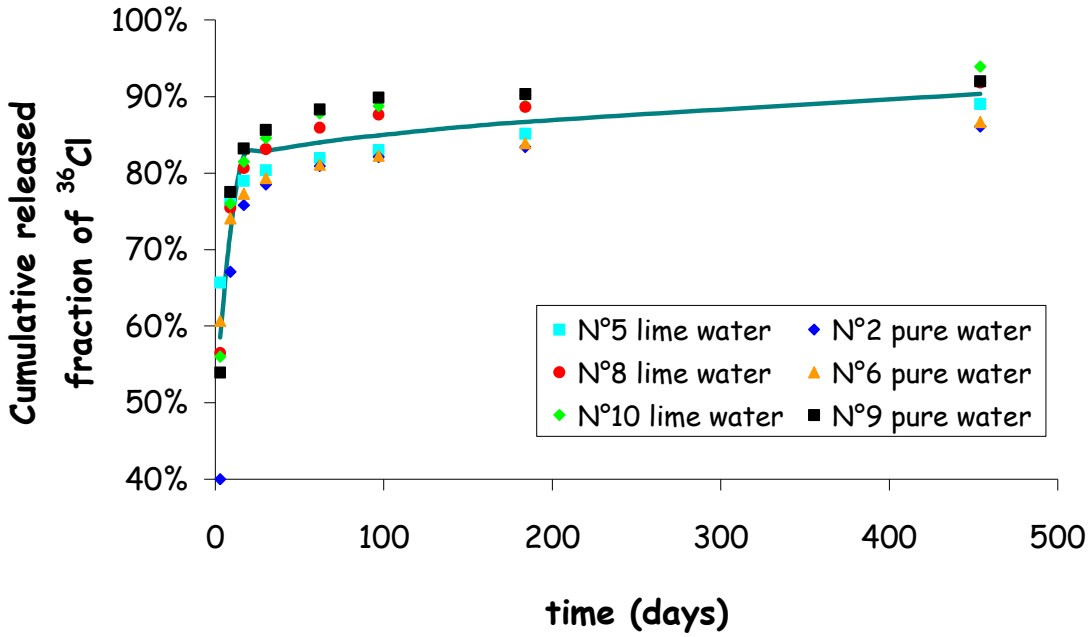

Figure 17 - Chlorine 36 released fraction and computed diffusion profile (solid line) in pure water.

Two diffusion coefficients were fitted in line with sites 1 and 2. Values are shown in Table 11 for G2 and Bugey 1 graphite. The effective diffusion coefficient is calculated from (6:

$$D_e = \theta . D_a \ (\theta = 0.2 \text{ is the graphite porosity}) \qquad (6)$$

Table 11 - Diffusion coefficients fitted from tests on G2 and Bugey 1 graphite samples.

	Site 1 D_a (m^2/s)	Site 1 D_e (m^2/s)	Site 2 D_a (m^2/s)
G2	$2{,}5.10^{-11}$	5.10^{-12}	$1{,}5.10^{-13}$
Bugey	4.10^{-12}	8.10^{-13}	6.10^{-14}

The diffusion coefficient values for G2 and Bugey 1 graphite samples are similar.

Chlorine diffusion tests were performed on non-irradiated graphite as well. A 1.8cm-thick sample from G2 reactor was placed between two tanks between which a constant concentration gradient was imposed. The effective diffusion coefficient is calculated from the amount of ^{36}Cl crossing the sample over time. In steady-state conditions, equation (7)**(7** is applied:

$$Q = \frac{D_e C_0}{L} t - \frac{\alpha L C_0}{6} \quad (7)$$

where

Q: amount of ^{36}Cl that crosses the sample per surface unit (Bq/m^2)

De: effective diffusion coefficient (m^2/s)

C_0: initial concentration (Bq/m^3)

L: sample thickness (m), $\alpha = \theta + (1 - \theta)\tilde{\rho}K_d$,

θ: material porosity

ρ: graphite density

K_d: retention coefficient for the element in the material.

Figure 18 plots the QL/C0 ratio versus time. The slope gives the effective diffusion coefficient De = 4.10-12 m^2/s.

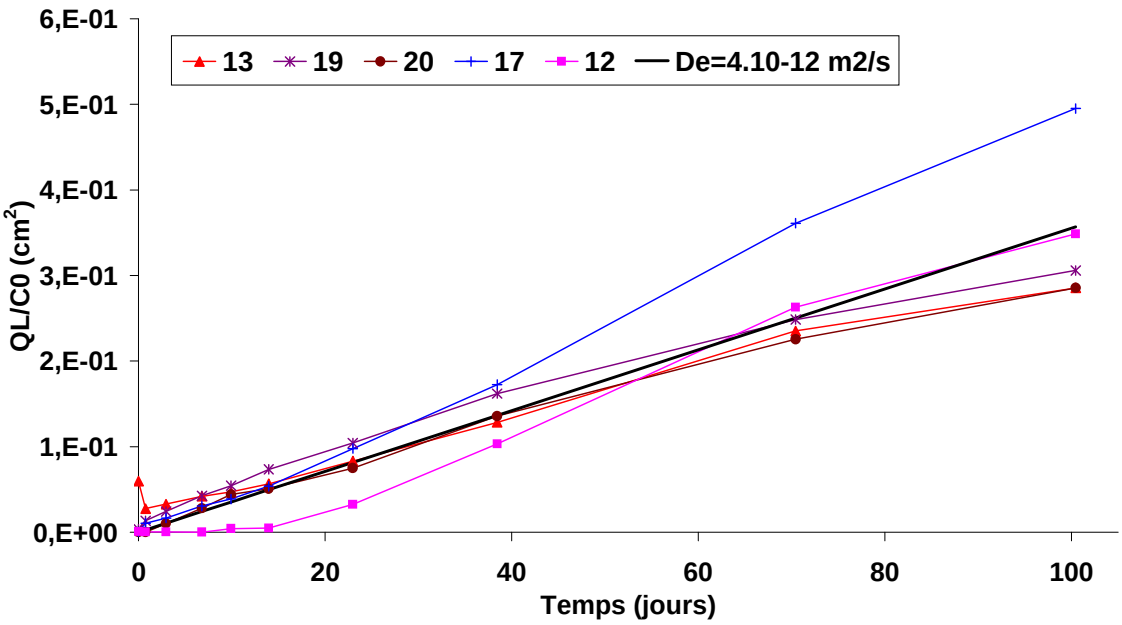

Figure 18 - ^{36}Cl diffusion through a sample of non-irradiated G2 graphite.

This is in agreement with values listed in Table 11. Similar diffusion tests were conducted on non-irradiated graphite from Bugey 1, and they provide the same value: $D_e = 5.10^{-12}$ m^2/s.

4.2.6 Conclusion on the behavior of ^{36}Cl

The release of chlorine-36 from irradiated graphite samples shows characteristic features:

- the samples dimensions play an important role in chlorine release into solution. It is consistent with a diffusion-driven mechanism.
- for Bugey 1 samples, the position of graphite within the stack- and thus its thermal history - has a strong influence on chlorine release: the higher the operating temperature, the lower the chlorine release. This behavior could be related to carboxyhydrogenated deposits formed in the graphite porosity and on the surface that could prevent or slow down the chlorine 36 release in solution.
- For G2 samples, released fractions were all similar whatever the leaching medium (UP water or lime water).
- For G2 samples, more than 80% of the initial amount of chlorine 36 is leached within the first month. The residual fraction is released much more slowly. To explain the release kinetics of ^{36}Cl, the presence of two forms of chlorine 36 has been assumed [30]: a major fraction (≈ 80%) weakly bound to graphite, and a complementary fraction that is strongly bound to graphite and/or located in the graphite infraporosity. Fit on experimental values based on a diffusion model seems to confirm the presence of two forms of chlorine.
- The diffusion of chlorine 36 in non-irradiated and irradiated graphite from G2 and Bugey 1 reactors was also studied with diffusion cells. Effective diffusion coefficients were calculated and they are consistent with leaching data: $D_e = 5.10^{-12}$ m^2/s.

4.3 Behavior of ^{3}H and ^{14}C

4.3.1 Comparison of results for G2 and Hanford reactors

4.3.1.1 Results from the PNL

Results for ^{14}C release are summarized in Table 12 after 90 days of leaching for G2 samples and 56 days for Hanford samples [24,25].

Table 12 shows that the amount of ^{14}C released in solution is very low (<1%) for both reactors, even though G2 samples show a greater release of ^{14}C than the Hanford samples.

Table 12 –Cumulative leached fraction of ^{14}C for G2 (1988) and Hanford (1987) graphite samples (PNL results)

Reactor	N°	Medium, T(°C)	V_L/S (cm)	V/S (cm)	Graphite mass (g)	A_0 (kBq/g) ^{14}C	F (%) ^{14}C
Hanford (PNL)	DIW25	Water, 25	9.25	0.5	40	260	0.009*
	DIW50	Water, 50					0.018*
	DIW90	Water, 90					0.050*
	HGW25	Groundwater, 25					0.004*
	HGW90	Groundwater, 90					0.026*
G2 (PNL)	2	Water, 20				16.3	0.85
	13					53.9	0.26
	14					65.3	0.33

* at 56 days

4.3.1.2 Results from the CEA laboratory

Results are presented in Table 18 after 90 days of leaching. Both ^{3}H and ^{14}C are studied.

Table 13 – Cumulative leached fraction of ^{3}H and ^{14}C for G2 (09/01/1988) and Hanford (06/24/1989) samples (CEA results).

Reactor	N°	Medium, T(°C)	V_L/S (cm)	V/S (cm)	Graphite mass (g)	A_0 ^{14}C (kBq/g)	F (%) ^{14}C	A_0 ^{3}H (kBq/g)	F (%) ^{3}H
Hanford (CEA)	D1	Water, 23	10	1.26	650	230	0.0006	885	0.0009
	E2					170	0.0004	636	0.0014
	G3					170	0.0004	500	0.0018
G2 (CEA)	2					6.1	0.003	382	2.8
	13					18.6	0.0006	367	0.035
	14					23.3	0.0004	345	0.15
	12			0.55	50	18.3	0.36	-	-
	15					17.4	0.08	-	-

Tritium activities and release rates are more or less the same for both reactors.

For ^{14}C, initial activities measured by the PNL and the CEA are comparable. In both tests, Hanford samples have an initial activity in carbon-14 that is ten times as high as G2 samples. Among G2 samples, core n°2 logically shows the lowest initial activity in ^{14}C as it comes from G2 reflector, and it has thus experienced a lower neutron flux than the moderator. Cumulative released fractions of ^{14}C measured by the CEA on G2 samples (cores n° 2, 13 and14) are lower than that from PNL, but they are similar for cores n° 12 and 15 for which a leakproof reactor

was used. It suggests that ^{14}C may have escaped as gaseous species (CO_2 or CO) from cores n° 2, 13 and 14.

4.3.2 Leaching on G2 graphite stack

Results for G2 stack samples are shown in Table 14 after 97 days of leaching [31].

Table 14 – Cumulative leached fraction of ^{14}C and ^{3}H for G2 stack samples (03/09/2004). Values in blue are below the detection limit.

Reactor	N°	Medium, T(°C)	V_L/S (cm)	V/S (cm)	A_0 ^{14}C (kBq/g)	F (%) ^{14}C	A_0 ^{3}H (kBq/g)	F (%) ^{3}H
G2 Core n°36	2	UP water, 20	2.2	0.576	8.6	<0.028	36	<0.040
	6		2.4	0.511	20	<0.018	38	0.031
	9		2.2	0.576	25	0.027	49.2	0.078
	5	Lime water, 20	2.4	0.511	13	<0.02	44	<0.019
	8		2.2	0.576	18	0.02	48	<0.004
	10		2.2	0.576	31	0.014	55	<0.021

On the whole, ^{14}C and ^{3}H show a low leaching rate (<0.1%), and lots of values are below the detection limit (in blue in Table 14). After 465 days of leaching, the maximum value is found for tritium, with a cumulative leached fraction of 0.4% (not shown in Table 14).

There is no difference between values in lime water and in pure water. This is in agreement with the leaching tests on Bugey 1 graphite as reported below.

Measurements of ^{3}H release in the gas phase were also performed after 97 days of leaching for samples n°2 and 6. They show a low fraction of tritiated water (HTO) in the vapor phase with respect to that found in solution. Thus, there is no significant release of gaseous tritium during leaching tests.

4.3.3 Graphite leaching on Bugey 1 stack

Leaching results for Bugey 1 stack samples are shown in Table 15 after 90 days of leaching [28,29]. Both solid and powder samples are studied.

For tritium, release rates are low, with the exception of sample N86 whose leached fraction reaches 3.19%. They show neither medium (lime *vs.* pure water) nor temperature sensitivity. Influence of the sample form (solid *vs.* powder) is also negligible.

Table 15 - Cumulative leached fraction of ^{3}H and ^{14}C for Bugey 1 graphite on solid (09/17/2001) and powder (23/05/2006) samples. Values in blue are below the detection limit.

Reactor	N°	Medium, T(°C)	V_L/S (cm)	V/S (cm)	A_0 ^{14}C (kBq/g)	F (%) ^{14}C	A_0 ^{3}H (kBq/g)	F (%) ^{3}H
Bugey (block)	N55	Water, 20	1	0.33	8.3	<0.01	141	0.59
	N58				57	<0.001	25	0.12
	N75				8.5	<0.009	6.31	0.27
	N76	Water, 40			84	0.034	140	0.071
	N85				6.1	<0.016	362	0.438
	N86				33	0.009	352	3.19
	N57	Lime water, 20			100	0.0014	21	0.06
	N59				20	<0.005	270	0.004
	N98				30	<0.003	20	0.184
Bugey (powder)	N87	Water, 20	-	-	39	<0.035	36	0.07
	N67+N68				95	<0.06	22	<0.06
	N88				20	<0.06	6.8	<0.2

With the exception of samples N76, N86 and N57, ^{14}C released fractions are below the detection limit. They do not depend on the medium (lime *vs.* pure water), on the temperature nor on the sample form (solid *vs.* powder). For samples N76, N86 and N57, the release is higher but remains very low (< 0.04%).

Figure 19 shows the evolution of ^{14}C released fraction with time for Bugey 1 samples. Leaching results on G2 graphite stacks (see section 4.3.2) are also displayed for comparison.

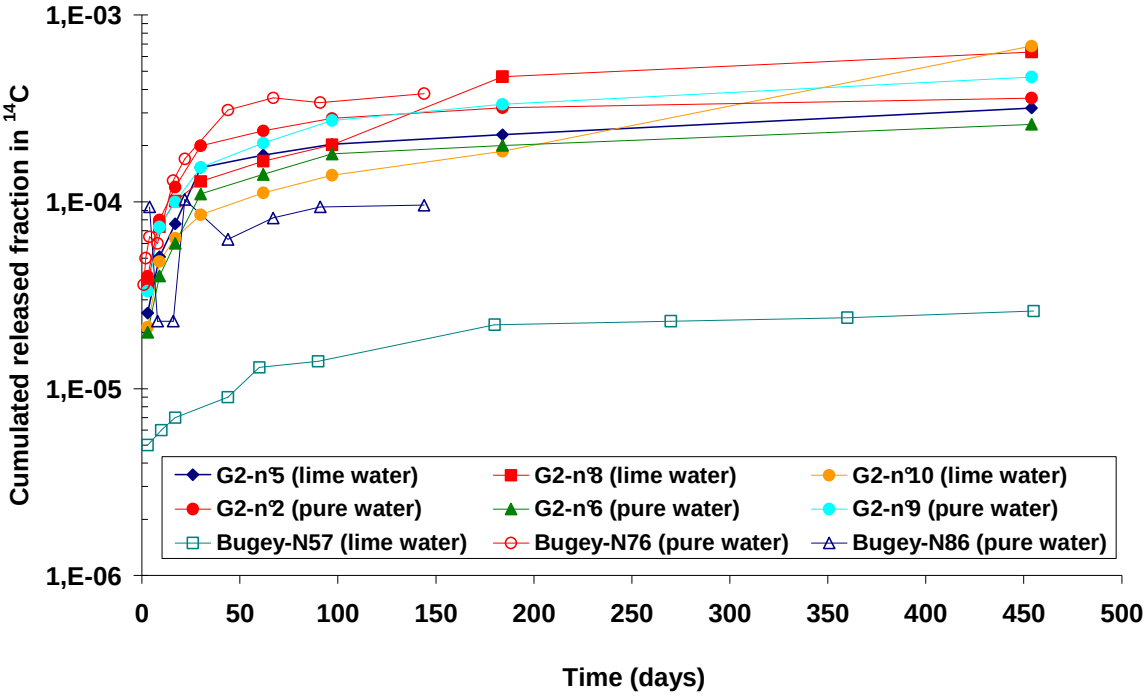

Figure 19 - Cumulative leached fraction of ^{14}C versus time for G2 and Bugey samples.

The ^{14}C release for Bugey 1 and G2 occurs in two steps:

- The initial release is rather rapid, and occurs within the first 90 days of leaching. It may arise from ^{14}C generated by activation of ^{14}N impurities from the coolant or activation of ^{13}C contained in the deposits.
- Subsequently, the ^{14}C release kinetics is very slow. It may come from ^{13}C activation in the bulk.

The ^{14}C dissolution rate was derived from G2 experiments and provided a value of 3.10^{-7} $g.m^{-2}.j^{-1}$. Fachinger et al. [32] measured the same value - 6.10^{-7} $g.m^{-2}.j^{-1}$ - for graphite oxidation in aqueous solution, suggesting that ^{14}C release roughly coincides with graphite oxidation.

4.3.4 Graphite leaching from SLA2 sleeves

Results of SLA2 sleeves leaching are collected in Table 16 after 90 days of leaching [27,28]. Tritium is the main radionuclide in the leachate but its release rate is fairly low with respect to the initial activity. It may be bound in a chemical form that limits its dissolution [28].

As already observed for G2 and Bugey leaching tests, ^{14}C release occurs in two steps: the initial release is rather fast (1.3 to 6.8% of the initial activity) while it significantly decreases

afterwards. Only the ^{14}C present on the graphite surface seems to be leached, while bulk ^{14}C is more stable and is released on the long run [28].

Table 16 - Cumulative leached fraction of ^{3}H and ^{14}C for SLA2 sleeves (07/18/2007).

Reactor	N°	Medium, T(°C)	V_L/S (cm)	V/S (cm)	Dose rate (µGy/h)	A_0 ^{14}C (kBq/g)	F (%) ^{14}C	A_0 ^{3}H (kBq/g)	F (%) ^{3}H
SLA	01	Water, 20	11.9	0.27	30	2.55	0.95	221	0.034
	07				120	3.93	1.46	580	0.014
	24				12	0.38	6.29	289	0.022

4.3.5 ^{3}H diffusion measurements in graphite

Diffusion tests were conducted on a thin sample of non-irradiated graphite (1.8 cm thick) from G2 reactor. The experimental procedure is similar to that applied for chlorine in section 4.2.5. The aim is to determine the ^{3}H diffusion coefficients within graphite. Figure 27 plots the QL/C_0 ratio versus time. The effective diffusion coefficient is measured from the slope value, and gives 6.10^{-12} m^2/s. This is in agreement with tests on non-irradiated graphite from Bugey reactor: De = 1.10^{-11} m^2/s.

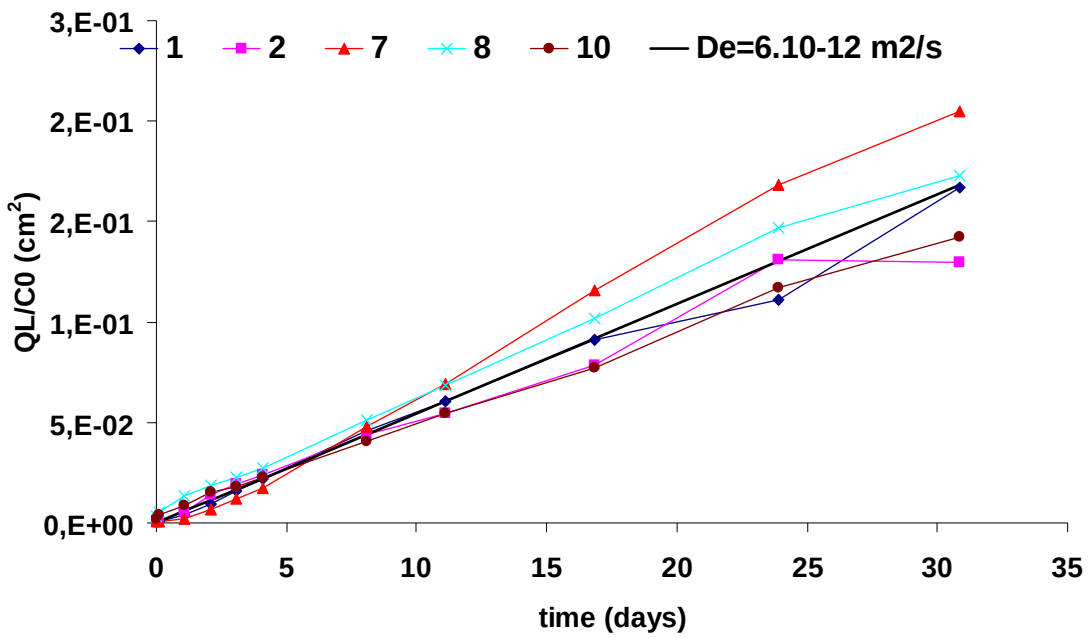

Figure 20 - Tritium diffusion through a sample of non-irradiated graphite from G2 reactor.

4.3.6 Conclusion on ^{3}H and ^{14}C leaching behavior

The release of tritium and carbon-14 from irradiated graphite is small whatever the sample origin, but the initial activities are far more important than chlorine-36. Leaching rates depend neither on the temperature nor on the leaching medium.

It can be assumed that only ^{14}C on graphite surface generated by neutron activation of ^{14}N impurities or ^{13}C in the deposits is leached. The major part of remaining ^{14}C is formed from bulk ^{13}C and is released on the long run, together with graphite oxidation. Tests will be conducted in France to improve knowledge on ^{14}C behavior.

The diffusion coefficient of tritium through a thin sample of non-irradiated graphite has been measured in a diffusion cell. Values for G2 and Bugey 1 samples are 7.10^{-12} m^2/s and 1.10^{-11} m^2/s respectively.

4.4 Behavior of other radionuclides

4.4.1 Graphite leaching on G2 stack

Results on G2 stack are collected in Table 17 after 97 days of leaching. The release of ^{60}Co, ^{63}Ni, ^{133}Ba and ^{137}Cs was followed [31].

Table 17 - Cumulative leached fraction of ^{60}Co, ^{63}Ni, ^{133}Ba and ^{137}Cs for G2 stack samples (03/09/2004)

Reactor	G2, Core n°36					
Medium, T(°C)	UP water, 20			Lime water, 20		
N°	2	6	9	5	8	10
A_0 ^{60}Co (kBq/g)	0.45	1.45	1.72	1.42	1.52	1.51
F (%) ^{60}Co	6	9.2	8.6	0.5	0.3	0.4
A_0 ^{63}Ni (kBq/g)	3.06	4.88	6.45	6.54	6.24	5.34
F (%) ^{63}Ni	1.2	2.8	2.5	0.5	0.4	0.5
A_0 ^{133}Ba (Bq/g)	25	26	25	28	26	26
F (%) ^{133}Ba	12	11	8.6	20.1	10	5.2
A_0 ^{137}Cs (Bq/g)	37	63	76	66	73	85
F (%) ^{137}Cs	8.2	10	9.5	11.6	8	5.1

^{133}Ba and ^{137}Cs behave similarly: 5 to 20 % of cesium and barium atoms are released into solution after 97 days of leaching. Such values do not change significantly after 455 days of leaching. The chemical composition of the solution has no effect.

In contrast, the release of nickel and cobalt atoms is pH-sensitive. In pure water, the cumulative leached fractions range from 1.2 to 2.8 % for ^{63}Ni and from 6 to 9.2 % for ^{60}Co. In lime water, release rates decrease down to 0.5 % for both ^{63}Ni and ^{60}Co. This is in line with the precipitation of cobalt and nickel atoms under alkaline conditions (lime water).

4.4.2 Graphite leaching from Bugey 1 stack

4.4.2.1 Block samples

The release of ^{60}Co, ^{137}Cs and ^{63}Ni was studied for Bugey 1 stack samples. Results are shown in Table 18 after 90 days of leaching [29].

Table 18 - Cumulative leached fraction of ^{60}Co, ^{137}Cs and ^{63}Ni from Bugey 1 stack block samples.

Reactor	N°	Medium, T(°C)	A_0 ^{60}Co (kBq/g)	F (%) ^{60}Co	A_0 ^{137}Cs (Bq/g)	F (%) ^{137}Cs	A_0 ^{63}Ni (kBq/g)	F (%) ^{63}Ni
Bugey	N55	Water, 20	9.62	20.3	-	-	10.9	12
	N58		131	2.3	-	-	92.4	0.2
	N75		35.1	17.8	-	-	23.7	19.2
	N76	Water, 40	40.5	0.95	98	18.4	58.1	0.17
	N85		5.19	1.20	583	0.36	7.29	1.0
	N86		15.4	1.25	699	15.4	14.1	0.74
	N57	Lime water, 20	79.2	0.15	143	0.002	72	0.07
	N59		1.9	0.045	-	-	46.2	0.325
	N98		61	0.004	-	-	76	0.06

^{60}Co and ^{63}Ni behave in the same way. Surprisingly enough, their release rates decrease with increasing temperature [29]. As for G2 samples, they significantly decrease by a factor of 100 in alkaline solution whatever the leaching time. This is probably due to the precipitation of cobalt and nickel atoms which may have been enhanced by the partial renewal of the leachate.

4.4.2.2 Powder samples

^{60}Co, ^{133}Ba, ^{134}Cs, ^{137}Cs, ^{154}Eu and ^{155}Eu leaching was studied on Bugey 1 stack powder samples. Results are given in Table 19 after 90 days of leaching [29].

Table 19 - Cumulative leached fraction of ^{60}Co, ^{133}Ba, ^{134}Cs, ^{137}Cs, ^{154}Eu and ^{155}Eu from Bugey 1 stack powder samples (05/23/2006).

Reactor	**Bugey (powder)**		
Medium, T(°C)	**Water, 20**		
N°	N87	N67+N68	N88
A_0 ^{60}Co (kBq/g)	39	9.1	36
F (%) ^{60}Co	9	59	37
A_0 ^{133}Ba (Bq/g)	<57	190	<39
F (%)^{133}Ba	-	34	-
A_0 ^{134}Cs (Bq/g)	84	100	190
F (%)^{134}Cs	31	-	18
A_0 ^{137}Cs (Bq/g)	107	<45	<41
F (%)^{137}Cs	33	-	-
A_0 ^{154}Eu (Bq/g)	<28	422	<30
F (%)^{154}Eu	-	74	-
A_0 ^{155}Eu (Bq/g)	<39	200	<40
F (%)^{155}Eu	-	75	-

^{60}Co release in solution is fast and occurs within the first month. Values are quite variable as they range from 9 to 59% of the initial activity.

For other isotopes, the released fractions range from tens to hundreds of Bq/g. The major part of the release occurs during the first sampling sequence (1 month). Yet, it is difficult to draw conclusions regarding the behavior of ^{133}Ba, ^{134}Cs, ^{137}Cs, ^{154}Eu and ^{155}Eu as most of measurements are below the detection limit.

4.4.3 Graphite leaching from SLA2 sleeves

Radionuclides studied for graphite leaching experiments on SLA2 sleeves are ^{60}Co and ^{137}Cs. Results are presented in Table 20 after 90 days of leaching [27,28].

Table 20 - Cumulative leached fraction of ^{60}Co and ^{137}Cs for SLA2 sleeves (07/18/1997).

Reactor	N°	Medium, T(°C)	V_L/S (cm)	V/S (cm)	Dose rate (µGy/h)	A_0 ^{60}Co (kBq/g)	F (%) ^{60}Co	A_0 ^{137}Cs (Bq/g)	F (%) ^{137}Cs
SLA	01	Water, 20	11.9	0.27	30	2.8	0.38	21.6	36.0
	07				120	2.6	2.28	11.4	69.4
	24				12	1.4	1.41	2.7	87.0

^{60}Co is an activation product and is hardly released in solution.

In contrast, ^{137}Cs is almost fully leached, which may be due to [28]:

- Its origin: it is a fission product and is thus mainly found on graphite surface. Contamination can come either from the rupture of the fuel cladding or from the decladding pools where fuel assemblies are stored.
- Its chemical behavior: it is highly soluble in water.

4.4.4 Conclusion on the behavior of other radionuclides

The release of ^{60}Co from graphite is very low with the exception of leaching tests on powder. ^{60}Co and ^{63}Ni release is significantly reduced under alkaline conditions probably because of the precipitation of cobalt and nickel hydroxides.

^{137}Cs within SLA2 sleeves is significantly released which may be explained by its highly soluble chemical form.

5 Conclusion

The available leaching data on French and American graphite provide a good basis for assessing important trends and raising issues on radionuclides release. More specifically, three typical leaching trends can be pointed out.

^{60}Co and ^{63}Ni release into solution is rather limited, and is especially slowed down in alkaline solution because of the precipitation of cobalt and nickel hydroxides.

^{14}C is the main long-lived radionuclide in French graphite waste but its release in solution is quite slow. ^{14}C release occurs in two steps, which may be related to the ways of production of ^{14}C in nuclear reactors. The ^{14}C that is initially released may arise from activation of either the ^{14}N impurities adsorbed on to graphite surface or of the ^{13}C atoms contained in carboxyhydrogenated deposits. The residual ^{14}C inventory is generated by activation of the ^{13}C atoms in the bulk and is released on the long run congruently with the graphite matrix dissolution. The speciation of ^{14}C released from graphite is not characterized yet but studies are underway in France.

Uncertainties mainly concerns ^{36}Cl whose leaching behavior is still confusing. It is currently believed that chlorine release occurs in two steps along with two forms of chlorine:

- the initial “spike” release – up to 80% of the total chlorine inventory - may correspond to chlorine atoms that are weakly bound to graphite or located in the graphite macroporosity. The evolution of the cumulative leached fraction and tests in diffusion cells indicate that such a release is a diffusion-driven process.
- the residual chlorine fraction is non labile and is released very slowly. It is assumed to be strongly bound to graphite and/or located in graphite infraporosity.

The presence of two forms of chlorine has been recently observed by XPS and TDP techniques[5] on non-irradiated graphite samples by the Nuclear Physics Institute in Lyon (IPNL, [33]). More generally, research is carried out to investigate this non-labile fraction and to identify mechanisms that are rate-determining for its release. This program is partly included in Carbowaste actions and gathers EDF, Andra and several French research institutes (CEA, IPNL, ENS-Paris, Subatech). Three processes are under study:

[5] XPS : X-rays photoelectron spectroscopy ; TDP : temperature programmed desorption

- Water penetration into graphite. Water penetration may restrain chlorine release, especially as graphite is hydrophobic. It also strongly depends on graphite porosity and microstructure which are thus studied as well.
- Chlorine solubilization. Chlorine chemical form may be partially insoluble, so its speciation is studied using various spectroscopic techniques and thermal treatments.
- Chlorine leaching kinetics. Chlorine release may be considerably slowed down by the presence of surface deposits. Chlorine may also be located within graphite closed porosity where water hardly penetrates.

Another significant result is the large dispersion on ^{36}Cl leached fractions, *i.e.* large dispersion on the chlorine labile fraction. Such a dispersion seems to be related to the position of graphite samples within reactor stacks. New experiments have confirmed this result and showed the correlation between sample thermal history in reactor and the ^{36}Cl leached fraction.

For the time being, the only practical consequences that can be deduced from these results are that the bulk of ^{14}C located in the graphite matrix is quite stable, and will be steadily released on the long run. Only the ^{14}C located on the crystallite surface is easily released by leaching. In contrast, chlorine atoms are expected to be strongly released during underwater dismantling, so that a large part of the chlorine inventory may be trapped into ion exchange resins. For graphite waste dismantled under dry conditions, chlorine release will occur as soon as water penetrates waste packages.

There are still uncertainties on leaching results, and it is not expected that future works will significantly modify release models under disposal conditions. In this regard, conservative assumptions have to be made in particular for chlorine-36 whose inventory is considered to be fully released upon contact with water. In France, this has led Andra to define a minimum clay thickness of 50 meters for the design of a shallow disposal facility for graphite waste. This geological barrier should secure radionuclides migration and delay their discharge to the biosphere.

6 References

[1] Pichon, C. 2008. Comportement des radionucléides dans les graphites UNGG en milieu aqueux – Synthèse bibliographique et proposition de programme, Technical Report, NT SA3C/LARC 08-02, CEA.

[2] Berenger, F. 2007. Projet graphite – Document de base – Connaissance générale des réacteurs », Technical Report, NT ELIER0700644, EDF.

[3] Bonal, J.P. ; Robin, J. 2006. Un matériau fascinant : le graphite, Monographie de la Direction de l'Energie Nucléaire « Les réacteurs nucléaires à caloporteur gaz », CEA.

[4] Rappeneau, J. 1961. Effets des rayonnements des piles sur le graphite, Technical Report, DPC/PCA/SPMN/61-92, CEA.

[5] Rappeneau, J. 1960. Effets des rayonnements sur les piles de graphite, Technical Report, DPC/PCA/60-1067/JR/JB, CEA.

[6] Rappeneau, J. 1966. Variations dimensionnelles des graphites sous l'effet des rayonnements neutroniques, BISTn°105.

[7] Bonal, J.P.2002. Les dépôts sur les empilements des réacteurs UNGG, Technical Report, DMN/SEMI/LM2E/RT/02-10, CEA.

[8] Brié, M. 1990. Mesure de la teneur en eau et de la cinétique de reprise d'humidité des carottes de graphite de BUGEY1, Technical Report, DTA/DIR.90.NT.02, CEA.

[9] CEA. 1966. Corrosion radiolytique du graphite, DPC/SPCA.

[10] Oxydation radiolytique du graphite. Interprétation des résultats d'analyses du gaz caloporteur dans les centrales EDF1 et EDF2, X MP.6, 1967.

[11] Bresard, I.; Bonal, J.P. 2000. *Caractérisations mécanique, chimique et radiologique du graphite des réacteurs de la filière UNGG*, DEN Editions.

[12] Blanchard, R.; Brisbois, J.; Koch, C. 1971. Oxydation du graphite et dépôts hydrogénés dans le réacteur BUGEY1, Technical Report, SERMA. 15/71. DMG. 37/71, CEA.

[13] Beck, K. 2006. Etude des propriétés hydriques et des mécanismes d'altération de pierres calcaires à forte porosité. Ph.D. diss., Orléans Univ., France.

[14] Yvars, M.; Mottet, P.; Sailleau, J. 1965. Etude des graphites artificiels polycristallins par microscopie optique, Technical Report, PCA/SPMN/65.300, CEA.

[15] 1966. Effet WIGNER dans le graphite, DPC/PCA/SPMN, CEA.

[16] Hering, H. 1955. Effet des neutrons rapides sur le graphite, Lessons of atomic engineering 2nd eds. 1955-1956.

[17] Mottet, P.; Yvars, M.; Gerlinger, P. 1968. Détermination des densités réelles des graphites nucléaires. Influence de l'irradiation neutronique sur la microporosité et les variations dimensionnelles, Technical Report, n° 666 DPC/PCA/SPMN/68-239, CEA.

[18] Yvars, M.; Mottet, P.; Sailleau, J. 1969. Effets des rayonnements neutroniques sur la porosité des graphite, Technical Report, n° 400 DPC/PCA/SPMN/66-30, CEA.

[19] Bonal, J.P. 1999. Estimation de l'état de l'empilement de graphite du réacteur BUGEY 1 après 50 ans de confinement, Technical Report, SEMI/LM2E/RT/99-019/A, CEA.

[20] Lang, F.M.; Lafargue, Y. 1968. Différents états du système eau-carbone. Cas des graphite poreux. *CR.Acad.Sc.*266.

[21] Brié, M. 1992. Evaluation de l'oxydation de l'empilement de graphite du réacteur SAINT LAURENT A1 après 50 ans de confinement, Technical Report, DTA/DIR 92 NT 04, CEA.

[22] Chenion, J. 1974. Méthode et appareillage originaux conçus pour étudier l'interaction de la vapeur d'eau sur les matériaux. Application au bilan des produits hydrogénés fixés et désorbés du graphite à différentes températures. Ph. D. diss., Paris VI Univ., France.

[23] Lang, F.M.; Magnier, P.; Valle, C.; Cazard, J.1965. Physisorption et chimisorption de l'eau par le graphite nucléaire. In Proceedings of the 7th Conference on Carbon.

[24] Gray, W.J.; Morgan, W.C. 1989. Leaching of ^{14}C and ^{36}Cl from irradiated French graphite, Technical Report, PNL-6989, Pacific Northwest Laboratory.

[25] Gray, W.J.; Morgan, W.C. 1988. Leaching of ^{14}C and ^{36}Cl from Hanford Reactor Graphite, Technical Report, PNL-6769, Pacific Northwest Laboratory.

[26] Costes, J.R.; Vidal, H.; Raymond, A.; Révy, D. 1992. Report following the agreement for the exchange of irradiated graphite samples and leaching data between the United States Department of Energy and the Commissariat à l'Energie Atomique, DCC/UDIN 92/223.

[27] Parraud, S. 1999. Lixiviation de chemises de graphite de St Laurent A, résultats définitifs », Technical Report, NT SCCD 99-15, CEA.

[28] Parraud, S. 2003. Lixiviation du graphite des chemises du réacteur UNGG de St Laurent A, Technical Report, NT SAMRA 02-043, CEA.

[29] Simondi-Teisseire, B.; Senes, S.; Combes, C. 2003. Lixiviation des empilements graphite de Bugey, Rapport final, Technical Report, NT SAMRA 03-027, CEA.

[30] Comte, J. 2006. Lixiviation des poudres d'empilements de graphite de Bugey, Analyses Report n°SA3C/LARC 2004/0329 of June 9 2006, CEA.

[31] Guy, C.; Comte, J.; Combes, C.; Senes, S.; Thouvenin, M. 2007. Lixiviation des empilements graphite de G2, comportement des radio-nucléides, Technical Report, NT SA3C/LARC 07-02-ind.0, CEA.

[32] Fachinger, J.; den Exter, M.; Grambow, B.; Holgersson, S.; Landesman, C.; Titov, M.; Podruhzina, T. 2006. Behaviour of spent HTR fuel elements in aquatic phases of repository host rock formations. *Nuclear Engineering and Design* 236: 543-554.

[33] Vaudey, C. E.; Toulhoat, N.; Moncoffre, N.; Bérerd, N.; Favergeon, L.; Pijolat, M.; Raimbault, L.; Sainsot, P.; Rouzaud, J. N. 2008. Thermal behavior of chlorine in nuclear graphite. In Proceedings of the 9th International Nuclear Graphite Specialists Meeting, oral communication.